Published in final edited form as:
Inorg Chem. 2011 October 17; 50(20): 9804–9815. doi:10.1021/ic200783a.

A Study of Mo(4+)Quinoxalyl-Dithiolenes as Models for the Non-Innocent Pyranopterin in the Molybdenum Cofactor

Kelly G. Matz[1], **Regina P. Mte**[2], **Rebecca Rothstein**[1], **Martin L. Kirk**[2,*], and **Sharon J. Nieter Burgmayer**[1,*]

[1]Department of Chemistry, Bryn Mawr College, Bryn Mawr, Pennsylvania 19010

[2]Department of Chemistry and Chemical Biology, The University of New Mexico, Albuquerque, New Mexico 87131-0001

Abstract

A model system for the molybdenum cofactor has been developed that illustrates the non-innocent behavior of a N-heterocycle appended to a dithiolene chelate on molybdenum. The pyranopterin of the molybdenum cofactor is modeled by a quinoxalyl-dithiolene ligand (S_2BMOQO) formed from reaction of a molybdenum tetrasulfide and a quinoxalyl alkyne. The resulting complexes TEA[Tp*MoX(S_2BMOQO)] (**1**, X = S; **3**, X = O; TEA = tetraethylammonium; Tp* = hydro*tris*(3,5-dimethylpyrazolyl)borate) undergo a dehydration-driven intramolecular cyclization within the quinoxalyl-dithiolene forming Tp*MoX(pyrrolo-S_2BMOQO) (**2**, X= S; **4**, X= O). **4** can be oxidized by one electron to produce the Mo(5+) complex **5**. In a preliminary report of this work evidence from X-ray crystallography, electronic absorption and resonance Raman spectroscopies, and DFT bonding calculations revealed that **4** possesses an unusual asymmetric dithiolene chelate with significant thione-thiolate character. The results described here provide a detailed description of the reaction conditions that lead to formation of **4**. Data from cyclic voltammetry, additional DFT calculations and several spectroscopic methods (infrared, electronic, resonance Raman, electron paramagnetic resonance) have been used to characterize the properties of members in this suite of five Mo(S_2BMOQO) complexes and further substantiate the highly electron-withdrawing character of the pyrrolo-S_2BMOQO ligand in **2** and **4**. This study of the unique non-innocent ligand S_2BMOQO provides examples of the roles that the N-heterocycle pterin can play as an essential part of the molybdenum cofactor. The versatile nature of dithiolene appended by heterocycles may aid in modulating the redox processes of the molybdenum center during the course of enzyme catalysis.

Introduction

Metal complexes with dithiolene ligands were first investigated during the 1960's[1] and due to their many unusual properties they remain the focus of study fifty years later. Metal-dithiolenes have significant roles in biological catalysis[2,3] and in materials research,[4–8] especially electronics and sensor applications.[9,10] Progress made in detailing the electronic structure of metal dithiolenes has been a vehicle to understand their unusual properties. The highly covalent metal-dithiolene unit posseses flexible redox behavior that facilitates intramolecular metal-ligand redox processes.[11] As such, dithiolene ligands exhibit "non-innocent" behavior and metal-dithiolenes are among a limited number of inorganic systems that display extensive metal-ligand redox interplay making them useful as key components of donor-acceptor molecules.[12,13] From a valence bond perspective, dithiolene ligands can be viewed as existing somewhere between the extremes of the neutral dithione/dithiete and

sburgmay@brynmawr.edu, mkirk@unm.edu.

dianionic dithiolate ligand forms. (Fig. 1). This description is distinct from the formal oxidation state behavior observed for their dioxolene ligand complexes, which display a well-behaved quinone–semiquinone–catecholate series with discrete oxidation states being assigned to the ligand and the metal.[14] The principal difference between dianionic and neutral dithiolene ligands is the number of π electrons present in the S-C=C-S backbone of the dithiolene. For the neutral dithiones, the S=C-C=S fragment possesses four π electrons and for the dianionic form there are six π electrons.

Our curiosity about molybdenum dithiolenes originates from our query into their partnership with pterins in the pyranopterin molybdenum enzymes.[2] Pterins possess multiple redox states accessed through complicated redox proceses and, like dithiolenes, have been shown to be non-innocent redox partners with metals.[15–19] For example, reduced pterins chelated to Mo at the O4, N5 site can generate three resonance structures where the electron density shifts from a deprotonated tetrahyropterin to the Mo atom resulting in three valence tautomeric structures in Scheme 1.[20]

The Mo-pterin-dithiolene structure found at the catalytic active site (Fig. 2) within pyranopterin molybdenum enzymes creates the most redox rich unit known in bioinorganic chemistry. The molybdenum atom participates in two-electron redox chemistry coupled to formal oxygen atom transfer, the dithiolene has the capability of two electron oxidation to a dithione and the pyranopterin unit can potentially participate in multi electron transfer. In addition, the redox chemistry of pterins is necessarily associated with proton transfer, presenting further opportunities to the protein to induce non-innocent behavior at the molybdenum cofactor controlled through H-bonding between the pyranopterin and nearby protein residues. Several groups have speculated on possible ways that the pyranopterin dithiolene ligand might be an active component of the catalytic reaction.[21–23] Possible roles include participation as electronic conduit between the molybdenum center and other electron transfer units in the protein and as a switch to adjust the Mo redox potential. Credence for these speculations has been provided by several recent X-ray structures that show the pyran ring of the dithiolene ligand on Moco can exist in both the closed pyrano-form as well as the open, non-cyclized form.[24–26]

Because it is difficult to directly study the behavior of the pyranopterin dithiolene in Moco while bound within the protein, we have turned to small molecule analog studies to obtain such information. Our strategy for exploring the possibilities created by a Mo-pterin-dithiolene partnership has been to develop the reaction chemistry of pterin- and quinoxaline-substituted dithiolene complexes of molybdenum to serve as small molecule analogues for studying the effects of these N-heterocycles on dithiolene properties.[27]

In a recent Communication we reported the unusual electronic structure exhibited by an oxo-Mo(4+)-quinoxaline-substituted dithiolene complex, $Tp^{*}Mo^{4+}(O)$(pyrrolo-S_2BMOQO) (Tp* is hydro*tris*(3,5-dimethylpyrazolyl)borate) containing a rare thiolate-thione ligand.[28] This compound exhibits a remarkable donor-acceptor character that affects the Mo(5+/4+) redox couple and beautifully illustrates the potentially non-innocent role of a N-heterocycle, such as a pterin, in modulating molybdenum redox potentials during the course of pyranopterin molybdenum enzyme catalysis. Here we describe in more detail the synthesis, reaction chemistry and properties of other members of the S_2BMOQO family of quinoxalyl-dithiolene complexes of molybdenum: TEA[$Tp^{*}Mo^{4+}(S)(S_2$BMOQO)] **1**, $Tp^{*}Mo^{4+}(S)$(pyrrolo-S_2BMOQO) **2**, TEA[$Tp^{*}Mo^{4+}(O)(S_2$BMOQO)] **3**, $Tp^{*}Mo^{4+}(O)$(pyrrolo-S_2BMOQO) **4** and [$Tp^{*}Mo^{5+}(O)$(pyrrolo-S_2BMOQO)]Cl **5**.

Experimental Section

Materials and Methods

All syntheses were conducted under anaerobic atmosphere using standard Schlenk techniques unless otherwise noted. Solvents were dried over activated molecular sieves overnight to remove residual water. 2-Chloroquinoxaline was purchased from Sigma-Aldrich and purified by sublimation using a McCarter vacuum apparatus. TEA[Tp*$Mo^0(CO)_3$] (Tp* is hydro*tris*(3,5-dimethylpyrazolyl)borate; TEA^+ is tetraethylammonium) was prepared following the method of Curtis and Shiu[29] then thoroughly washed with methanol to remove residual water, ether, and hexanes before drying under vacuum. TEA[Tp*$Mo^{IV}S(S_4)$] was prepared by a slight adaptation of a previously reported procedure[30] where activated 3 Å molecular sieves replace alumina. NMR spectra were obtained from a Bruker 300 MHz or Varian INOVA 500 MHz instrument. Infrared spectra were collected on a Perkin-Elmer Model 2000 FT-IR Spectrometer from samples prepared as KBr pellets. ESI-MS spectra were obtained on a Waters Micromass ZQ. High resolution ESI-MS (HRESI-MS) were obtained by Dr. Somogyi on an Ion Spec Fourier Transform Mass Spectrometer. Samples for mass spectral analysis were dissolved in acetonitrile under aerobic conditions and directly injected, bypassing the liquid chromatography column.

UV-Vis data were obtained on a Beckman DU 800 Spectrophotometer. Electrochemical analyses were performed using a BioAnalytical Systems CV50 system, using TBAP (tetrabutylammonium perchlorate) as electrolyte in acetonitrile, platinum working and auxiliary electrodes and Ag/AgCl as reference electrode. All potentials are referenced to an internal ferrocene potential (+0.40 V vs. Ag/AgCl).

Synthesis. 2-(3-Butynyl-2-methyl-2-ol) quinoxaline (BMOQO)

$Cl_2Pd(PPh_3)_2$ (0.1130 g, 0.1610 mmol) in triethylamine (100 mL) and DMSO (40 mL) was stirred under nitrogen for ten minutes. The solution was stirred for ten min after each addition of the remaining reagents: copper iodide (0.0307 g, 0.1612 mmol), 2-chloroquinoxaline (2.240 g, 0.01360 mol) and 2-methyl-3-butyn-2-ol (1.3 mL, 0.01341 mol). Stirring six hours at room temperature caused the triethylamine layer to become bright yellow while the DMSO layer containing the catalysts and product turned dark brown. The reaction flask was briefly chilled at 4 deg C (45 min) to freeze the brown DMSO layer. The triethylamine layer was decanted and discarded. Distilled water (100 mL) was added to the frozen DMSO layer, and the thawed mixture was poured into a separatory funnel. The organic layer was extracted with dichloromethane, washed three times with 30 mL portions of distilled water, and the water layer was back extracted with three 30 mL portions of dichloromethane. The organic layers were combined and washed twice with 20 mL portions of saturated aqueous NaCl before they were dried over magnesium sulfate. After filtering to remove the $MgSO_4$, the CH_2Cl_2 solution containing BMOQO was rotary evaporated to produce a light brown solid, which was dried under vacuum overnight. A tan solid was obtained in 91 % yield (2.624 g, 0.01232 mol). **^{1}H NMR ($CDCl_3$)**: δ (ppm): 8.88 (1H, s, quin *H*3), 8.12-8.08 (2H, m, Ar*H*), 7.83-7.76 (2H, m, Ar*H*), 2.28 (1H, s, O*H*), 1.70 (6H, s, C-CH_3). **ESI-MS** (CH_3CN): m/z: $[M]^{—}$: 212.

TEA [Tp*Mo^{IV}(S)(S_2BMOQO)] 1

Acetonitrile (40 mL) was transferred to a flask containing TEA[Tp*$Mo^{IV}(S)(S_4)$] (0.2170 g, 0.3168 mmol) and BMOQO (0.0672 g, 0.3169 mmol). The reaction was stirred at room temperature for 4 h, and then chilled in the freezer overnight. The mixture was filtered, and the filtrate was evaporated to 10 mL. Cold, de-aerated ether (50 mL) was added, and the mixture was chilled in the freezer for 2h to promote product precipitation. Filtration of the

solvent yielded a dark, plum-colored solid in 90% yield (0.2376 g, 0.285 mmol). **^{1}H NMR ($CDCl_3$)**: δ (ppm): 9.92 (1H, s, quin *H*3), 8.21-7.50 (4H, Ar*H*), 5.92 (1H, s, Tp* pyrazolyl-*H*), 5.90 (1H, s, Tp* pyrazolyl-*H*), 5.41 (1H, s, Tp* pyrazolyl-*H*), 2.90 (3H, s, C-CH_3), 2.42 (3H, s, C-CH_3), 2.29 (6H, s, Tp* pyrazolyl-CH_3), 2.28 (3H, s, Tp* pyrazolyl-CH_3), 2.22 (3H, s, Tp* pyrazolyl-CH_3), 2.18 (3H, s, Tp* pyrazolyl-CH_3), 2.02 (3H, s, Tp* pyrazolyl-CH_3). **IR** (KBr-disk): ν(B-H): 2520 cm^{-1}; ν(Mo=S): 496 cm^{-1}. **ESI-MS** (CH_3CN): m/z: [M−]: 703.0, $[M+TEA]^+$: 833, observed as Mo^{5+}; $[M+2TEA]^+$: 963, observed as Mo^{4+}. **HRESI-MS** *m/z* [M−]: 703.1171 (calcd for (M−) 703.117032 M = C28H34ON8S3BMo).

Tp*Mo^{IV}(S)(pyrrolo-S_2BMOQO) 2

A 40 mL portion of acetonitrile was de-aerated over activated alumina for twenty minutes, then transferred to a deaerated Schlenk flask containing TEA[Tp*Mo(S)S_4] (0.217 g , 0.391 mmol) and BMOQO (0.083 g, 0.390 mmol). The reaction was heated to 70 °C for 4 h then cooled to room temperature before it was placed in the refrigerator overnight. The dark mixture was filtered, then the filtrate was concentrated under vacuum on the Schlenk line. Deaerated diethylether was added to the residue, the flask was placed in the refrigerator for 2 h. The crude product was isolated by filtration yielding a shiny black solid (2.41 g, 3.51 mmol). Purification of **2** is done on a short, fast-running silica gel column. Any TEA[Tp*Mo(O)S_4] contaminant elutes first with dichloromethanthane then 2 is eluted with 2–5% MeOH/CH_2Cl_2 as a bright blue band. ^{1}H NMR: δ (ppm), 9.62 (1H, s, quin *H*3), 8.21-7.30 (4H, Ar*H*), 6.15 (1H, s, Tp* pyrazolyl-*H*), 6.12 (1H, s, Tp* pyrazolyl-*H*), 5.25 (1H, s, Tp* pyrazolyl-*H*), 3.07 (3H, s, cyclized C-CH_3), 3.05 (3H, s, cyclized C-CH_3), 2.63 (3H, s, Tp* pyrazolyl-CH_3), 2.60 (3H, s, Tp* pyrazolyl-CH_3), 2.18 (3H, s, Tp* pyrazolyl-CH_3), 2.12 (3H, s, Tp* pyrazolyl-CH_3), 2.10 (3H, s, Tp* pyrazolyl-CH_3), 1.74 (3H, s, Tp* pyrazolyl-CH_3). IR (KBr disk), cm^{-1}: ν(C=O, C=N): 1541, 1443, 1438, 1412, 1380, 1365; ν(Mo=S): 523. ESI^+MS: m/z: $[M^+]$: 686 as Mo(5+). **HRESI-MS** *m/z* [M+]: 686.1126 (calcd for (M) 686.1132 M = C28H33BN8S3Mo).

TEA [Tp*Mo^{IV}(O)(S_2BMOQO)] 3

TEA [Tp*Mo^{IV}(S)(S_2BMOQO)] (0.2000 g, 0.2401 mmol) and triphenylphosphine (0.0786 g, 0.300 mmol) were stirred under nitrogen in 'wet' acetonitrile (~2% H_2O) (30 mL) at room temperature for one hour. The mixture was then filtered to remove excess triphenylphosphine, and the filtrate was reduced under vacuum to 5 mL. De-aerated ether (40 mL) was added, and the flask was placed into the freezer overnight. The ether was filtered to yield a dark, purple-red solid in 98 % yield (0.1920 g, 0.235 mmol). **^{1}H NMR ($CDCl_3$)**: δ (ppm): 9.95 (1H, s, quin *H*3), 8.11-7.43 (4H, Ar*H*), 5.95 (1H, s, Tp* pyrazolyl-*H*), 5.93 (1H, s, Tp* pyrazolyl-*H*), 5.44 (1H, s, Tp* pyrazolyl-*H*), 2.88 (6H, s, C-CH_3), 2.73 (3H, s, Tp* pyrazolyl-CH_3), 2.35 (3H, s, Tp* pyrazolyl-CH_3), 2.30 (6H, s, Tp* pyrazolyl CH_3), 2.16 (3H, s, Tp* pyrazolyl-CH_3), 2.08 (3H, s, Tp* pyrazolyl-CH_3). **IR** (KBr-disk): ν(B-H): 2530 cm^{-1}; ν(Mo=O): 914 cm^{-1}. **ESI-MS** (CH_3CN): m/z: $[M]^-$: 687, $[M+TEA]^+$: 817, observed as Mo(5+); $[M+2TEA]^+$: 947, observed as Mo(4+). **HRESI-MS** *m/z* [M−]: 687.1400 (calcd for (M−) 687.139876 M = C28H34O2N8S2BMo).

Tp*Mo^{IV}(O)(pyrrolo-S_2BMOQO) 4

Tp*Mo(S)(pyrrolo-S_2BMOQO) (0.200 g, 0.291 mmol) was dissolved in 30 mL acetonitrile. An excess of triphenylphosphine (0.079 g, 0.300 mmol) was added and the solution stirred for one hour at room temperature. The solution was then concentrated under vacuum, and ether was added to yield a dark blue precipitate in 97% crude yield. The product was chromatographed on neutral alumina using 5% methanol/dichloromethane. ^{1}H NMR: δ (ppm), 9.52 (1H, s, quin *H*3), 8.22-7.62 (4H, Ar*H*), 6.00 (1H, s, Tp* pyrazolyl-*H*), 5.98 (1H, s, Tp* pyrazolyl-*H*), 5.43 (1H, s, Tp* pyrazolyl-*H*), 2.81 (3H, s, cyclized C-CH_3), 2.79 (3H, s, cyclized C-CH_3), 2.45 (6H, s, Tp* pyrazolyl-CH_3), 2.29 (6H, s, Tp* pyrazolyl-CH_3), 2.21

(3H, s, Tp* pyrazolyl-C*H*$_3$), 1.80 (3H, s, Tp* pyrazolyl-C*H*$_3$). ^{13}C{H} NMR: δ (ppm), 146 (C3), 133 (C7, C8), 128, 114 (C6, C9), 108, 107, 106 (3 *C*H-pyrazole), 17, 16, (−*C*H$_3$, BMOQO), 13, 12 6 (−*C*H$_3$, pyrazole). IR (KBr disk), cm^{-1}: ν(C=O, C=N): 1541, 1443, 1438, 1412, 1380, 1365; ν (Mo=O): 922. ESI$^+$MS: m/z: [M+]: 670.0, observed as Mo(5+). **HRESI-MS** *m/z* [M+]: 670.1383 (calcd for (M) 670.136039 M = C28H33BON8S2Mo).

[Tp*Mo^V(O)(pyrrolo-S$_2$BMOQO)]Cl 5

A 0.050 g sample of blue Tp*Mo^{IV}(O)(pyrrolo-S$_2$BMOQO) was dissolved in 10 mL of acetonitrile. A 0.5 mL aliquot of 3% hydrogen peroxide was added, and the reaction immediately turned cherry-red. The sample was then washed with a saline solution, resulting in a bright pink acetonitrile layer and providing the chloride counterion to precipitate the complex. Addition of hexanes resulted in precipitation of red, microcrystalline **5** in 92% yield. IR (KBr-disk): **ν**(Mo=O): 935 cm^{-1}. ESI$^+$MS: m/z: [M+]: 670.0. **HRESI-MS** *m/z* [M +]: 670.1377 (calcd for (M) 670.136039 M = C28H33BON8S2Mo).

Reactivity studies

Experiments on the reactivity of complexes **1** – **4** used ESI-MS to monitor the change in species distribution as the solution environment was varied. Samples were dissolved in either acetontrile or CH_2Cl_2. Studies on the effect of dehydrating agents used microwave-activated 3 Å molecular sieves or alumnina.

EPR Spectroscopy

EPR spectra were collected at X-band (9.3 GHz) using a Bruker EMX spectrometer with associated Bruker magnet control electronics and microwave bridges. Low-temperature were collected in dichloromethane, and the temperature was controlled using an Oxford Instruments liquid helium flow cryostat. Simulations of the EPR spectra were performed using the program X-Sophe and the matlab toolbox EasySpin.[31]

Electronic Absorption Spectroscopy

Electronic absorption spectra were collected using a Hitachi U-3501 UV–Vis–NIR dual-beam spectrometer capable of scanning a wavelength region between 185 and 3200 nm. The electronic absorption spectra were measured in a 1-cm pathlength, 100 μL, black-masked, quartz cuvette (Starna Cells, Inc.) equipped with a Teflon stopper. All electronic absorption spectra were collected at room temperature and repeated at regular time intervals to ensure the stability and integrity of the sample in solution.

Raman Spectroscopy

Solid state resonance Raman (rR) spectra and associated rR excitation profiles were collected using a system comprised of an PI/Acton SpectraPro SP-2556 500 mm focal length imaging spectrograph with a triple grating turret and a PI/Acton Spec-10:100B back-illuminated 1340 × 100 pixel digital CCD spectroscopy system with a cryogenically cooled camera head. A Coherent Innova Ar^+ ion laser was the excitation source. Samples were mixed with either NaCl or a NaCl/Na_2SO_4 mixture with Na_2SO_4 as an internal calibrant. Resonance Raman excitation profile were plotted using Kr^+ laser line at 647nm and Ar^+ laser lines at 458, 488 and 514 nm where all peaks were normalized with respected to 992 cm^{-1} Na_2SO_4 peak.

Computational Details

Electronic structure and vibrational frequency calculations were performed at the density functional level of theory using the Gaussian 03W software package (Gaussian 03, R. C. G., Inc., Pittsburgh, PA, 2003.). All calculations employed the B3LYP hybrid functional and

used a LANL2DZ basis set with an effective core potential for Mo. A 6–31G* basis set was used for all light atoms. Input files were prepared using the molecule builder function in the Gaussview software package. The starting geometries were those of complex **4**. All geometries were fully minimized in the calculations. Molecular orbitals were analyzed using the AOMix program.[32,33] Electron density difference maps (EDDMs) were constructed using the GaussSum suite of programs. EPR parameters were calculated at the DFT level using ADF2009.01.[34–42] EPR parameters were calculated at the DFT level using ORCA 2.7.0. The ZORA scalar relativistic Hamiltonian with relativistic corrections were incorporated self-consistently in the ORCA calculation.[43] Electronic absorption spectra were calculated using DFT (Swizard) program.

Results and Analysis

Synthesis

A coupling reaction between the quinoxalyl alkyne, BMOQO, and TEA[Tp*Mo(S)(S_4)] produces two types of molybdenum quinoxalyldithiolene complexes where the reaction temperature determines which species forms (Fig. 3). The reaction under room temperature conditions results in the formation of TEA[Tp*Mo(S)(S_2BMOQO)], **1**, containing a 1,2-substituted dithiolene complex (Fig. 3 (a)). Elevated reaction temperatures (60 – 80 ° C) cause an intramolecular cyclization that occurs subsequent to dithiolene ligand formation yielding Tp*Mo(S)(pyrrolo-S_2BMOQO) **2** (Fig. 3 (b)).

Complex **2** results from the net loss of the hydroxyl group from the α-C of the alkyl side chain on the S_2BMOQO dithiolene ligand followed by intramolecular cyclization forming a 5-membered pyrrole-like ring. A possible mechanism (Fig. 4) for the formation of this pyrrolo-dithiolene involves hydroxyl protonation followed by loss of water to produce a carbocation on the akyl group. When the quinoxaline group is oriented so that N1 is adjacent to this carbocation, C-N bond formation and intramolecular cyclization results in a pyrrole ring fused to the quinoxaline at positions 1 and 2 (Fig. 4). The proposed mechanism is supported by the observation that anhydrous conditions, produced by addition of drying agents like molecular sieves to solutions of **1**, favor the dehydration step and cause rapid cyclization to **2**. The thermal conditions favoring reaction (b) in Fig 3 likely facilitate quinoxaline rotation putting N1 in proximity to the carbocation. Removal of water appears to be the key condition favoring cyclization of complex **1** to **2**. The oxo analog of the tetrasulfide reagent, TEA[Tp*Mo(O)(S_4)], does not react with alkynes, as previously reported by us and others.[27,44] Therefore use of pure [Tp*Mo(S)(S_4)]¯ is essential to the isolation of clean sulfido complexes **1** and **2**.

Both sulfido complexes **1** and **2** can be converted to the oxo analogs TEA[Tp*Mo(O)(S_2BMOQO)] **3** and Tp*Mo(O)(pyrrolo-S_2BMOQO) **4**, respectively, using triphenylphosphine to faciltate sulfide ligand dissociation. The formation of [Tp*Mo(O)(S_2BMOQO)]¯ **3** (Eq 1) is best perfomed in ‘wet’ acetonitrile (~2% H_2O) since trace water inhibits the dehydration step in Fig. 4 and blocks intramolecular cyclization that would lead to the pyrrolo-quinoxalyldithiolene complex **4**.

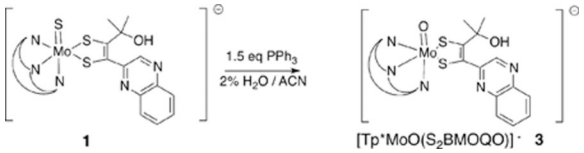

(Eq 1)

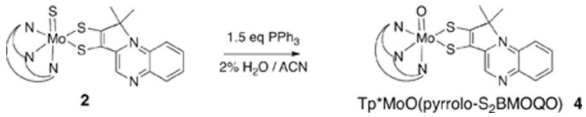

(Eq. 2)

The set of four BMOQO dithiolene complexes **1–4** exhibit a range of reactivities. $[Tp^{*}Mo(S)(S_2BMOQO)]^{-}$ **1** is stable as a solid in both aerobic and anaerobic conditions, however aerobic dissolution of **1** in a variety of solvents leads to both hydrolysis forming $[Tp^{*}Mo(O)(S_2BMOQO)]^{-}$ **3** and to cyclization reactions to yield a mixture of $Tp^{*}Mo(S)$(pyrrolo-S_2BMOQO) **2** and $Tp^{*}Mo(O)$(pyrrolo-S_2BMOQO) **4**. The progress of hydrolysis monitored by ESI-MS and proton NMR indicates that the *sulfido* dithiolene **1** hydrolyzes to form the *oxo* complex **3** slowly under anaerobic conditions (several days) when dissolved acetonitrile containing 2% water (v/v). Since under anaerobic conditions hydrolysis of the sulfido ligand in **1** is relatively slow, synthesis of **1** can be improved when performed in the presence of trace water since this condition inhibits the dehydration step and pyrrole ring closure while leaving the terminal *sulfido* ligand intact. The tendancy of **1** to dehydrate under anhydrous conditions means that ligand cyclization of **1** to form **2** is accelerated in the presence of molecular sieves. **1** does not survive purification by chromatography since both silica gel and alumina promote dehydration and formation of $Tp^{*}Mo(S)$(pyrrolo-S_2BMOQO) **2**, which can be visually identified by its vibrant blue hue. However this reactivity affords another method to prepare **2** through by column chromatography of **1**, in addition to the thermal reaction (Fig 3(b)). Plum-red $[Tp^{*}Mo(O)(S_2BMOQO)]^{-}$ **3** is the least robust of the four molybdenum dithiolenes. The complex is extremely unstable in solution, rapidly cyclizing to the $Tp^{*}Mo(O)$(pyrrolo-S_2BMOQO) **4** within minutes in air, after a few days under nitrogen atmosphere or by exposure to chromatographic silica or molecular sieves. The deep blue complex **4** is the most thermodynamically stable member of the four S_2BMOQO dithiolene complexes and **1, 2** and **3** all ultimately hydrolyze and cyclize to form **4**. The most direct and high yield preparative route to **4** is by thermal reaction of BMOQO and $[Tp^{*}Mo(S)(S_4)]^{-}$ to produce $Tp^{*}Mo(S)$(pyrrolo-S_2BMOQO) **2**, followed by hydrolysis in the presence of triphenylphosphine (Eq 1) and purification by chromatography on silica. We previously reported how **4** is oxidized by ferrocenium or hydrogen peroxide to the Mo(5+) complex $[Tp^{*}Mo(O)$(pyrrolo-S_2BMOQO)$]^{+}$ **5**. [16] The reaction is a striking one to observe visually as the intensely blue solution of **4** becomes bright cherry red on addition of oxidant as the Mo(5+) complex **5** forms. Solutions of **5** are not stable and they slowly revert to the Mo(4+) as indicated by color change to blue. Likewise, **5** cannot be chromatographed as it immediately turns blue on either silica or alumna support, again indicating return to the Mo(4+) oxidation. The greater stability of the Mo(4+) vs. Mo(5+) state is unique to the presence of the pyrrolo-quinoxaline-dithiolene ligand. All other known dithiolene complexes coordinated to the Tp*Mo(O) unit are isolated in the Mo(5+) state.

^{1}H and ^{13}C NMR Spectroscopy

Proton NMR spectral data were obtained for all four dithiolene complexes **1 – 4** confirming the diamagnetic character of the Mo(4+) formal oxidation state. The complexity of the proton NMR spectra is a reflection of the low C_1 symmetry of these complexes. Those protons most useful for distinguishing among the four complexes are quinoxaline H3 and the pyrazole ring protons. Quinoxaline H3 appears as a singlet far downfield, remote from all other protons, and is a useful diagnostic of the cyclized or non-cyclized state of the dithiolene. The two complexes with ‘open’ dithiolene ligands, **1** and **3**, exhibit H3 downfield at 9.92 and 9.95 ppm, a shift of >1 ppm from the H3 in the parent alkyne BMOQO (8.88

ppm). For **2** and **4** having pyrrolo-dithiolene ligands, H3 appears at 9.62 and 9.52 ppm. The absence of symmetry in the four complexes makes each pyrazolyl ring proton unique in the spectral region 5–6 ppm, however all four complexes share a pattern where two of the three pyrazolyl protons have chemical shifts near ~5.9 ppm and one proton occurs at a higher field resonance near 5.4 ppm. This pattern likely reflects the similar environment of the two pyrazole rings that flank the dithiolene and the unique environment of the pyrazole ring trans to Mo=X. ^{13}C NMR spectra were obtained only for **4** due to the limited solution stability of complexes **1 – 3**. Assignments for the carbon atoms in **4** were made by comparison to reported data for related quinxaline molecules.[45]

Vibrational Spectroscopy

Vibrational spectroscopy is a useful tool for the identification of Mo≡X (X = S, O) groups and monitoring the electronic environment at Mo, since these vibrational markers correlate with a change in formal oxidation state of the Mo center. Mo≡O stretching frequencies are related to the strength of the π-donor ability of the dithiolene ligand mediated by the sulfur donor atoms. Electron-rich dithiolene ligands donate electron density via their sulfur donor atoms into vacant Mo dπ orbitals (e.g. d_{yz} in Fig. 5). This π donation is in competition with the π-donation from the terminal oxo ligand and results in lower ν(Mo=O) stretching frequencies with increased S→Mo charge donation. Conversely, electron-withdrawing substituents on dithiolenes result in increased ν(Mo≡O) stretching frequencies due to poorer S→Mo charge donation. Although the Mo d_{x2-y2} orbital is non-bonding with respect to the terminal oxo donor see Fig. 5), dithiolene → Mo d_{x2-y2} charge donation leads to a reduction of the metal effective nuclear charge for d^0 Mo(6+) and d^1 M(5+) complexes. This in turn leads to a decrease in the ionic character of the Mo≡O bond and a corresponding decrease in ν(Mo≡O) stretching frequencies. Mo(4+) monooxo complexes possess a d^2 electron configuration with the d_{x2-y2} orbital being doubly occupied, and this results in no net charge transfer between the dithiolene and the Mo d_{x2-y2} orbital[46]. The correlation between ν(Mo≡O) energy and the electronic character of the ligands on the complex has been studied extensively.[47–49]

Table 1 lists data illustrating these trends for complexes **1 – 5** reported in this work in comparison to data from related Tp*Mo(=X)-dithiolene compounds. The Mo=O and Mo=S stretching frequencies observed for complexes 1– 5 are consistent with those observed in previously reported pterin-dithiolene complexes and other Tp*Mo(=X) (X = O,S) dithiolene complexes where generally, the ν(Mo=X) frequency shifts to higher energy on oxidation of Mo(4+) to Mo(5+)

A comparison between the Mo≡X (X= O,S) complexes **1 – 5** and the recently reported pterin dithiolenes[27] TEA[Tp^*Mo^{4+}(X)(S_2DIFPEPP)] and Tp^*Mo^{5+}(X)(S_2DIFPEPP) (S_2DIFPEPP = 1,2,-(2,4-difluorophenyl)(pterinyl)dithiolene) illustrates the electronic effects of dithiolene ligands on Mo≡O and Mo=S stretching frequencies. For oxo-Mo complexes of both pyrrolo-S_2BMOQO and S_2DIFPEPP dithiolenes, the Mo≡O stretching frequency shifts 13 and 7 cm^{-1}, respectively, to higher energy as the formal Mo oxidation state increases from +4 to +5. The effect of dithiolene substituents on $\nu_{Mo\equiv O}$, can be evaluated by comparing data for S_2BMOQO complexes **3** and **4** with that for TEA[Tp^*Mo^{4+}(O)(S_2DIFPEPP)].

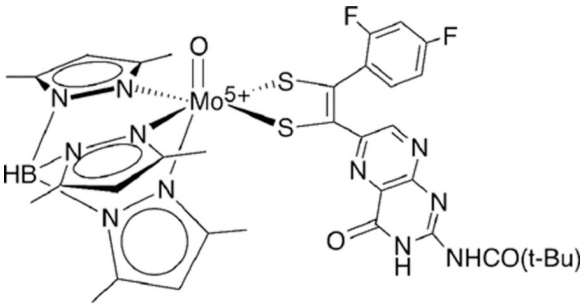

Tp*MoO(S_2DIFPEPP)

Comparison of $\nu_{Mo\equiv S}$ in **1** and **2** and $\nu_{Mo\equiv O}$ in **3** and **4** indicates that cyclization of the S_2BMOQO ligand to pyrrolo-S_2BMOQO causes an increase in $\nu_{Mo\equiv S}$ and $\nu_{Mo\equiv o}$ of 27 and 8 cm^{-1}, respectively, due to the electronic withdrawing effect of the conjugated pyrrolo-S_2BMOQO.

The B-H stretching vibration from the Tp^* ligand is also a reporter of electronic change or oxidation state at Mo. The data in Table 1 show that ν_{BH} shifts to higher energy by as much as 20 cm^{-1} on oxidation of Mo from +4 to +5. The electron withdrawing effect of the pyrrolodithiolene in **2** and **4** causes a considerably smaller increase in ν_{BH} of 6 and 8 cm^{-1}, respectively, when compared to the 'open' dithiolene complexes **1** and **3**.

EPR Spectroscopy of Tp*Mo^V(O)(pyrrolo-S_2BMOQO)$^+$ 5

Complex **5** can be readily obtained by hydrogen peroxide or iodine oxidation of **4** to yield the paramagnetic Mo(V) species. Room termperature and 75K EPR spectra for **5** are presented in Figure 6. A simulation of the isotropic spectrum yielded g_{iso} = 1.9672 and A_{iso} = 36.80 $\times 10^{-4}$ cm^{-1}. Spectral simulation of the anisotropic 75K data yielded spin-Hamiltonian paramters g_1 = 1.9966, g_2 = 1.9685, g_3 = 1.9389 (g_{ave} = 1.9678), and A_1 = 18 $\times 10^{-4}$ cm^{-1}, A_2 = 20 $\times 10^{-4}$ cm^{-1}, A_3 = 62 $\times 10^{-4}$ cm^{-1} (A_{ave} = 33 $\times 10^{-4}$ cm^{-1}).

Here, g_2 and A_2 are essentially coincident and lie along the molecular x-axis, while g_1, g_3, A_1 and A_3 are located in the molecular y-z plane with A_3 oriented very close to the Mo≡O bond. These values are typical of those found for neutral Tp*Mo^VO(dithiolene) compounds and compare quite favorably with the spin-Hamiltonian parameters that we, and others,[50] have obtained for Tp*MoO(bdt) (bdt = benzene-1,2-dithiolate) g_1 = 2.004, g_2 = 1.972, g_3 = 1.934 (g_3 = 1.970), and A_1 = 60 $\times 10^{-4}$ cm^{-1}, A_2 = 26 $\times 10^{-4}$ cm^{-1}, A_3 = 24 $\times 10^{-4}$ cm^{-1} (A_{ave} = 37 $\times 10^{-4}$ cm^{-1}). The only appreciable difference is a greater rotation of g_1 off of A_1 in **5** such that it is more closely oriented with A_3. We note in C_s Tp*MoO(bdt), which possess a y-z mirror plane, one component of the g-tensor and one component of the A-tensor (e.g. g_2 and A_2) are required to be coincident by symmetry. These results indicates that, for Tp* dithiolene systems, EPR spectroscopy does not appear to be a sensitive probe of overall complex charge (i.e. cationic vs. neutral), the charge on the dithiolene, or Mo-$S_{dithiolene}$ bond asymmetry as found in **5**.

Electronic Absorption Spectroscopy

A striking color change occurs upon cyclization of the open quinoxalyl-dithiolene ligands in complexes **1** and **3** to the cyclized pyrrolo-dithiolenes in **2** and **4**. Solutions of complexes **1** and **3** are both red-hued in color while pyrrolo-dithiolene complexes **2** and **4** are bright blue. In addition, **4** is solvatochromic and its low energy absorption undergoes bathochromic shifts of up to 55 nm. The rapid hydrolysis and cyclization reactions of **1** in solution have prevented acquisition of its electronic spectrum. The electronic absorption spectrum of

[TEA][Tp*Mo(O)(S_2BMOQO)]$^-$ **3** was obtained anaerobically in the presence of wet acetonitrile (2% H_2O) to prevent dithiolene cyclization and is presented in Figure 7. Complex **3** displays an absorption band at 500 nm (20,000 cm^{-1}), responsible for its red color and an intense higher energy absorption at 320 nm (31,250 cm^{-1}).

Both pyrrolo-dithiolene complexes **2** and **4** in acetonitrile are intensely blue due to strong abosorptions near 600 nm (~16,400 cm^{-1}). Figure 8 shows the spectrum of **2** (black line) and a spectrum of **4** (red line) generated in situ by hydrolysis of **2**. Remarkably, the 600 nm absorption band of **2** appears to display vibronic structure in solution with an apparent 1,250 cm^{-1} progression. On replacing the sulfido ligand by an oxo ligand, there is a large hypsochromic shift of 54 nm in the intense high energy absorption region of the spectrum (400 to 346 nm) while the low energy (~600 nm) absorption envelop of **2** displays a slight decrease in absorption intensity. We have previously reported the significance of the energy and intensity of the transition associated with the ~600 nm absorption of **4** and this transition has been assigned as an intraligand $S_{dithiolene}$ → quinoxaline charge transfer transition.[28] Since **2** exhibits the same ~600 nm absorption feature as **4**, we also assign this band in **2** also as an intralilgand $S_{dithiolene}$ → quinoxaline charge transfer transition. This assignment is corroborated by the results of time-dependent DFT calculations, and the intraligand nature of this transition in **2** is clearly evident in the calculated electron density difference map (EDDM) shown in Figure 9. The assignment of the ~600nm band in **2** can now be used to understand the electronic origin of the apparent vibronic structure observed for this band. Resonance Raman (rR) spectroscopy identified a number of high frequency quinoxaline vibrational modes in **4** that were strongly resonantly enhanced with excitation into the 16,400 cm^{-1} intraligand CT band. Most notable were resonantly enhanced intraligand vibrations that possessed dominant quinoxaline character (1345 cm^{-1}) and C=C plus quinoxaline character (1551 cm^{-1}). The ground state 1345 cm^{-1} in-plane quinoxaline stretch in **4** correlates very well with the 1,250 cm^{-1} excited state vibration in **2**, when one allows for an ~7% reduction in the ground state vibrational frequency. Low-termperature studies are planned to further address this issue.

Oxidation of **4** to **5** results in a shift of the intraligand CT band to higher energies (610 to 528 nm), while the UV absorption at 340 nm remains essentially unchanged (Figure 10). Oxidation of **4** does not seem to dramatically affect the nature of the intraligand CT band as observed in the calculated EDDM of **5** (Figure 11). However, the ~2,500 cm^{-1} increase in the energy of an intraligand transition upon oxidation of the metal ion deserves comment. It is well known that oxomolybdenum monodithiolenes undergo an increase in the folding of the dithiolene ligand with an increase in oxidation state.[51] The hole created in the Mo d_{xy} orbital upon one-electron oxidation of the corresponding Mo(4+) complex results in increased $S_{dithiolene}$→Mo d_{xy} charge donation that is facilitated by folding of the dithiolene ligand about the S---S vector (envelope fold). This has the effect of *stabilizing* the highest occupied dithiolene S orbital that is the donor orbital involved in the intraligand $S_{dithiolene}$ → quinoxaline charge transfer transition and *destabilizing* the Mo d_{xy} orbital. The net result is an energetic stabilization of the distorted (i.e. folded) Mo(5+) structure over the non-distorted structure, and a higher energy $S_{dithiolene}$ → quinoxaline charge transfer transition energy in oxidized **5** relative to reduced **4** (Figure 12).

The solution stability of Tp*Mo(O)(pyrrolo-S_2BMOQO) **4** and its solubility in solvents across a broad range of polarity permitted an investigation of its solvatochromic behavior. The low energy absorption of **4** occurs within the range 596 – 653 nm where, in solvents of high dielectric constant, the absorption envelope is centered at higher energies (~600 nm) while low dielectric solvents shift the absorption envelope to ~650 nm (Table 3). These observations are consistent with negative solvatochromic behavior for molecules having a polar ground state and nonpolar excited state.[m] A plot of absorption energy vs Lee's solvent

polarity constant E^*_{MLCT} has been shown to yield linear plots for MLCT in various types of complexes.[52] The fact that we observe a non-linear plot of the data in Table 3 may be interpreted as being consistent with the intraligand CT assignment for this low energy transition. Cummings and Eisenberg developed empirical solvent parameters[12] suitable for LLCT and use of these parameters (available for only the four solvents chloroform, acetone, toluene and dimethylsulfoxide) produced a plot of solvent parameter vs energy that had a higher linearity.

Cyclic Voltammetry

Three S_2BMOQO dithiolene complexes, **2, 3**, and **4**, were studied using cyclic voltammetry to compare their Mo(5+/4+) reduction potentials to those from other members of the Tp*Mo(X)(dithiolene) family. The data in Table 4 is referenced to the ferrocenium/ferrocene couple whereas the voltammograms in Figure 13 are plotted vs the potential of the reference electrode AgCl/Ag. The most stable member of this set, Tp^*Mo(O)(pyrrolo-S_2BMOQO) **4**, will be discussed first. The voltammogram of **4** displays two reversible redox couples (Figure 13, top) that have been assigned to the Mo (5+/4+) (−0.15 V) and pyrrolo-S_2BMOQO ligand reduction events (−1.25 V) based on comparison to related complexes (see below). In contrast, the 'open' dithiolene complex TEA[Tp^*Mo(O)(S_2BMOQO)] **3** displays a single reversible couple assigned to the Mo (4+/5+) couple (Figure 6, bottom) and lacks additional redox processes at negative potentials over the same potential window. The voltammogram of **3** shows two small couples (marked with *) at potentials characteristic of Tp^*Mo(O)(pyrrolo-S_2BMOQO) **4** and these provide additional evidence for the solution instability of **3** towards dehydration and intramolecular cyclization during the CV experiment.

The lack of a second reduction process indicates that the 'open', non-cyclized dithiolene ligand in **3** exhibits no ligand-based redox events in contrast to the redox active and reducible pyrrolo-dithiolene ligand in **4**. The Mo (4+/5+) couple in **3** is ~200 mV more negative than in **4** which implies that the pyrrolo-dithiolene ligand stabilizes the Mo(4+), a hypothesis consistent with it having appreciable electron withdrawing character. The sulfido pyrrolodithiolene complex **2** also exhibits both a Mo(5+/4+) and a ligand-based redox process and these two redox events occur at potentials more negative than those for the oxo complex **4**. The Mo(5+/4+) potential is 200 mV more negative in the sulfido complex **2** than in the oxo complex **4** while the pyrrolo-dithiolene ligand reduction is 330 mV more negative in **2** vs **4**.

The Mo (4+/5+) redox potentials of the S_2BMOQO dithiolene complexes are compared to those from other Tp*MoX(dithiolene) compounds in Table 4 and Figure 14. Table 4 compares data for **2, 3**, and **4** with reported data from pterin-dithiolene complexes of Tp*Mo(S,O). The Mo(5+/4+) potential is nearly identical for **3** and the pterin-dithiolene compounds indicating that, from an electronic structure point of view, there is little difference between a quinoxaline and a pterin substituent on a dithiolene ligand coordinated to Mo. Oxo molybdenum complexes **3** and **4** are compared to a broader range of Tp^*Mo(O)(dithiolene) compounds in Fig. 14 where the Mo(5+/4+) potential is plotted on an electrochemical 'yardstick'. Several striking points can be made from Fig. 14. First, the Mo(5+/4+) potential spans a range of more than one volt where the benzenedithiolate complex Tp*MoO(bdt) has the most negative value while the pyrrolo-dithiolene complex **4** has the most positive Mo(5+/4+) potential. Second, the electronic effect of the pyrrolo-dithiolene ligand in **4** can be ascertained as more electron withdrawing than the dimethylcarboxalate dithiolene (dmac) which is generally regarded as a very highly electron deficient dithiolene.[15] However, it should be noted that, in comparison to the anionic complex **3**, complex **4** is a neutral species and would be expected to have a favorable charge

effect on the reduction potential that contributes to a more stable reduced form of the Mo(5+/4+) couple.

Discussion

Five molybdenum dithiolene complexes TEA[Tp*Mo(S)(S_2BMOQO)] **1**, Tp*Mo(S)(pyrrolo-S_2BMOQO) **2**, TEA[Tp*Mo(O)(S_2BMOQO)] **3**, Tp*Mo(O)(pyrrolo-S_2BMOQO) **4** and [Tp*Mo(O)(pyrrolo-S_2BMOQO)]$^+$ **5** have been synthesized and characterized. The dithiolene ligand is generated during the synthesis of **1** by a coupling reaction of a quinoxalyl alkyne with a molybdenum tetrasulfide reagent, [TEA][Tp*Mo(S)(S_4)]. Complexes **1–3** are prone to two types of ligand-based reactions: (1) hydrolysis of the Mo=S unit in **1** and **2** to form the corresponding Mo≡O unit in **3** and **4** and (2) pyrrole ring formation following loss of the side chain hydroxyl group as water in **1** and **3** to yield **2** and **4**. Both of these reactions occur during chromatographic purification. During synthesis, however, the dehydration that precedes facile pyrrole ring closure can be controlled by adjusting the reaction environment. For example, the addition of 1–2% water to the reaction solvent prevents dehydration and pyrrole ring closure to favor formation of **1** and **3** whereas the addition of molecular sieves removes water and favors pyrrole ring formation to yield **2** and **4**. Surprisingly, the Mo=S group persists under conditions of trace water and is not hydrolyzed during the course of the reaction, indicating that the side chain hydroxyl is a more reactive site than the sulfido ligand with respect to hydrolysis. The irreversible nature of these two ligand reactions requires that reaction and isolation conditions for **1–3** must be carefully monitored to avoid their conversion to the most stable member of this set, Tp*Mo(O)(pyrrolo-S_2BMOQO) **4**.

We previously reported that an unusual electronic structure exists in dithiolene complex **4** based on results from X-ray crystallography, electronic spectroscopy, resonance Raman spectroscopy and DFT calculations.[28] The structure of the dithiolene chelate in **4** is asymmetric (Fig. 15a), where the two Mo-S and C–S bond distances differ by ~0.04 and 0.05 Å respectively. DFT calculations probing on the ground state and electronic transitions of **4** produced descriptions of the HOMO as primarily localized on the dithiolene sulfur atoms and the LUMO as predominantly quinoxaline-based. This led to an assignment of the intense visible absorption near 600 nm as intraligand dithiolene→quinoxaline charge transfer (ILCT) transition. Resonance Raman excitation profiles supported this assignment, since excitation into the intense 600 nm absorption results in resonantly enhanced quinoxaline vibrations between 1300 and 1500 cm^{-1}.[28] These results led to an interpretation of the electronic structure of the Mo-dithiolene as possessing thiolate-thione character contributed by resonance structure B in Fig. 15b. The partial oxidation of a thiolate to a thione illustrated in resonance structure B may be viewed as a consequence of the strong electron withdrawing effect of the pyrroloquinoxaline structure on the dithiolene. Data reported in this work (IR, CV, UV/vis) further support this strong electronwithdrawing effect and ILCT assignment. The Mo(5+/4+) potential for the pyrrolo-S_2BMOQO complex **4** is ~200 mV more positive than the non-cyclized -S_2BMOQO dithiolene complex **3** and this easier reduction of Mo is consistent with the shift of electron density from the Mo ion to the pyrrolo-quinoxaline mediated by the dithiolene chelate. Indeed, the Mo(5+/4+) potential in **4** at + 250 mV is the most positive redox potential ever found for a Tp*Mo(O)(dithiolene) species and explains to the exceptional stability of Mo(4+) in the class of Tp*MoO-dithiolenes typically most stable as (5+) complexes.

The proposed strong electronwithdrawing effect of the asymmetric thione-thiolate ligand is consistent with the dithiolene fold angle of ~14 ° in **4**. (Fig. 16). Dithiolene fold angles, i.e., the dihedral angle between planes formed by the M-S-S atoms and the S-C-C-S atoms, have been used as indicators to evaluate the extent of S(π p) → M(d) donation in metal

dithiolenes and dithiones. [53–57] Dithiolene and dithione folding increases with increasing oxidation state of the metal as a result of increased S(π p) → M(d) donation.[54,55] The metal ion in 4 is assigned a formal Mo(4+) oxidation and would be expected to exhibit a dithiolene fold angle near zero. The observed fold angle of ~14 ° in **4** corresponds to an intermediate value in the range observed for complexes of formal oxidation state Mo(4+) to Mo(5+). We interpret this result as indicative the electronic delocalization from the Mo(4+) ion to the pyrrolo-quinoxaline dithiolene ligand. Variation of dithiolene fold angle has been argued to potentially pay a role in electronic modulation within the Mo-pyranopterin dithiolene unit of Moco during catalysis.[53,58]

One other example of ditholene asymmetry in a Mo(4+) complex exists where the dithiolene ligand is also substituted by quinoxaline. $(Cp)_2$Mo(quinoxalyl-dithiolene) **6** (Eq. 3) possesses the same pyrrolo-dithiolene ring system as **2** and **4** and this dithiolene ligand is formed by a related reaction shown in Eq. 3. Electrophilic attack by the α-C atom is promoted by acid addition to a ketone precursor (Eq. 3).[59] A similar thione-thiolate electronic structure for the chelate can be inferred from the asymmetry in the S-C distances (S(1) – C(11) 1.706 Å vs S(2) – C(12) 1.762 Å) and from the intense low energy absorption (746 nm, 6900 M^{-1} cm^{-1}).

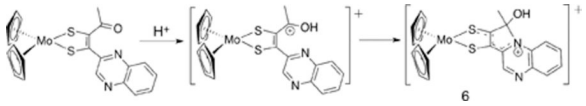

6

(Eq. 3)

Complexes **1** – **5** reported here provide new information on how N-heterocycles affect the electronic environments of Mo dithiolenes. Previous work has shown that protonation of quinoxalines and pyridines increases Mo redox potentials and that the basicity of N-cycles is increased (ΔpKa 1–3 units higher) when N-cycles are subsitutents on dithiolenes chelated to metals.[60] Increased basicity was attributed to resonance stabilization of the N-heterocycle through a contributing thione-thiolate resonance structure and analogous ILCT (dithiolene(S) → N-heterocycle) transitions were assigned.[60] Here we have described the conditions for a facile and thermodynamically favored intraligand cyclization that illustrates how reactions involving hydroxyalkyl substiuents on quinoxaline dithiolene ligands can be more favored than reaction at Mo=S. We have observed similar reactivity on pterin dithiolenes that will be reported later.

These studies provide examples of the roles that the N-heterocycle pterin can play as an essential part of the molybdenum cofactor (Moco). While pyrrole cyclization is not likely to have any role in the cofactor function, the electronic redistribution within the dithiolene chelate that results from electrophilic attack at pyrazine nitrogen does provide a valuable structural model for the consquence of protonation at pterin nitrogen atoms and this is illustrated in Figure. 17. Following pyrano ring opening in Moco, proton migration around the pyrazine ring of the pterin system accesses several different tautomers A – D, and one of those shown (D) possesses the asymmetric thione, thiolate chelate. Such a ring opening reaction of the pyranopterin has been documented in several enzymes.[24–26] The rearrangements in Figure 17 present an example of the electronic distribution consequences that may be operative in the enzymes. The results reported here provide evidence for the magnitude of the electronic effect of introducing thione, thiolate character into a dithiolene chelate on the redox potential of molybdenum.

Conclusion

The presence of the BMOQO dithiolene ligand in both oxo and relatively rare sulfido complexes of Mo(4+) alters the electronic properties of the overall molybdenum dithiolene complex, as shown through comparisons of these compounds to first-generation models such as $Tp^*Mo(O)(bdt)$, $Tp^*Mo(O)(tdt)$, and $Tp^*Mo(O)(qdt)$. This study points to a unique non-innocent ligand. The versatile nature of the BMOQO dithiolene unit may be relevant to the pterin dithiolene ligand found in Moco, as it is hypothesized the pyranopterin aids in modulating the redox processes of the molybdenum center during the course of enzyme catalysis.

Acknowledgments

MLK acknowledges the NIH (GM-057378) and the NSF (NSF CHE-0616190) for financial assistance. SJNB acknowledges the NIH (GM081848).

References

1. Stiefel EI, Eisenberg R, Rosenberg RC, Gray HB. J. Am. Chem. Soc. 1966; 88:2956–2966.
2. Burgmayer SJN. Prog. Inorg. Chem. 2004; 52:491–538.
3. Basu P, Burgmayer SJN. Coord. Chem. Rev. 2011; 255:1016–1038. [PubMed: 21607119]
4. Kirk ML, Helton ME, McNaughton RL. Prog. Inorg. Chem. 2004; 52:111–212.
5. Cassoux P, Valade L, Kobayashi H, Kobayashi A, Clark RA, Underhil AE. Coord. Chem. Rev. 1991; 110:115.
6. Faulmann C, Cassoux P. Prog. Inorg. Chem. 2004; 52:399–490.
7. Kato R, Liu YL, Aonuma S, Sawa H. Synthetic Metals. 1997; 86:2087.
8. Tanaka H, Okano Y, Kobayashi H, Suzuki W, Kobayashi A. Science. 2001; 291 285-).
9. Pilato RS, Van Houten KA. Prog. Inorg. Chem. 2004; 52:369–397.
10. Marbella L, Serli-Mitasev B, Basu P. Angew. Chem., Int. Ed. 2009; 48:3996–3998.
11. Eisenberg R, Gray HB. Inorg. Chem. 2011; 50:9741–9751. [PubMed: 21913669]
12. Cummings SD, Eisenberg R. J. Am. Chem. Soc. 1996; 118:1949–1960.
13. Zuleta JA, Bevilacqua JM, Rehm JM, Eisenberg R. J. Am. Chem. Soc. 1992; 31:1332–1337.
14. Pierpont C. Coord. Chem. Rev. 2001; 219–221:415–433.
15. Kaufmann HL, Liable-Sands L, Rheingold AL, Burgmayer SJN. Inorg. Chem. 1999; 38:2592–2599.
16. Burgmayer SJN, Arkin MR, Bostick L, Dempster S, Everett KM, Layton HL, Paul KE, Rogge C, Rheingold AL. J. Am. Chem. Soc. 1995; 117:5812–5823.
17. Fischer B, Straehle J, Viscontini M. Helv. Chim. Acta. 1991; 74:1544–1554.
18. Miyazaki S, Kojima T, Mayer JM, Fukuzumi S. J. Am. Chem. Soc. 2009; 131:11615–11624. [PubMed: 19722655]
19. Miyazaki S, Kojima T, Sakamoto T, Matsumoto T, Ohkubo K, Fukuzumi S. Inorg. Chem. 2007; 47:333–343. [PubMed: 18047328]
20. Burgmayer SJN, Kaufmann HL, Fortunato G, Hug P, Fischer B. Inorg. Chem. 1999; 38:2607–2613.
21. Enemark JH, Garner CD. J. Biol. Inorg. Chem. 1997; 2:817–822.
22. Burgmayer SNJ, Pearsall DL, Blaney SM, Moore EM, Sauk-Schubert C. JBIC, J. Biol. Inorg. Chem. 2004; 9:59–66.
23. Greatbanks SP, Hillier IH, Garner CD, Joule JA. J. Chem. Soc., Perkin Trans. 1997; 2:1529–1534.
24. Bertero MG, Rothery RA, Palak M, Hou C, Lim D, Blasco F, Weiner JH, Strynadka NCJ. Nat. Struct. Biol. 2003; 10:681–687. [PubMed: 12910261]
25. Jormakka M, Richardson D, Byrne B, Iwata S. Structure. 2004; 12(2004):95–104. [PubMed: 14725769]

26. Kloer DP, Hagel C, Heider J, Schulz GE. Structure. 2006; 14:1377–1388. [PubMed: 16962969]
27. Burgmayer SJN, Kim M, Petit R, Rothkopf A, Kim A, BelHamdounia S, Hou Y, Somogyi A, Habel-Rodriguez D, Williams A, Kirk ML. J. Inorg. Biochem. 2007; 101:1601–1616. [PubMed: 17765313]
28. Matz KG, Mtei RP, Leung B, Burgmayer SJN, Kirk ML. J. Am. Chem. Soc. 2010; 132:7830. [PubMed: 20481628]
29. Curtis MD, Shiu K. Inorg. Chem. 1985; 24:1213–1218.
30. Seino H, Arai Y, Iwata N, Nagao S, Mizobe Y, Hidai M. Inorg. Chem. 2000; 40:1677–1682. [PubMed: 11261979]
31. Stoll S, Schweiger A. J. Magn. Reson. 2006; 178:42. [PubMed: 16188474]
32. Gorelsky, SI. AOMix: Program for Molecular Orbital Analysis. Toronto: York University; 1997. http://www.sh-chem.net/.
33. Gorelsky SI, Lever ABP. J. Organomet. Chem. 2001; 635:187–196.
34. ADF2009.01 SCM, Theoretical Chemistry. Amsterdam, The Netherlands: Vrije Universiteit; http://www.scm.com
35. Gaussian 03. Pittsburgh, PA: R. C. G., Inc.; 2003.
36. Becke A. J. Chem. Phys. 1993; 98:5648.
37. van Lenthe E, van der Avoird A, Wormer PES. J. Chem. Phys. 1998; 108:4783.
38. vanLenthe E, Wormer PES, vanderAvoird A. J. Chem. Phys. 1997; 107:2488.
39. Neese, F. ORCA, an ab initio, density functional, and semi-empirical program package. Germany: University of Bonn;
40. Neese F. J. Chem. Phys. 2001; 115:11080.
41. Neese F. J. Chem. Phys. 2003; 119:9428.
42. Neese F. J. Chem. Phys. 2003; 118:3939.
43. Cauzzi D, Delferro M, Graiff C, Pattacini R, Predieri G, Tiripicchio A. Coord. Chem. Rev. 2010; 254:753–764.
44. Sproules SA, Morgan HT, Doonan CJ, White JM, Young CG. Dalton Trans. 2005:3552–3557. [PubMed: 16234937]
45. Bradshaw B, Collision D, Garner CD, Joule JA. Org. Biomol. Chem. 2003; 1:129. [PubMed: 12929399]
46. Bersuker, IB. Electornic Structure and Properties of Transion Metal Compounds. Introduction to the Theory. New York: Wiley-Interscience; 1996.
47. Chang CSJ, Enemark JH. Inorg. Chem. 1991; 30:683.
48. Garner CD, Hill L, Howlander NC, Hyde MR, Mabbs FE, Routledge VI, Less J. Common Mat. 1977; 54:27.
49. Helton ME, Gruhn NE, McNaughton RL, Kirk ML. Inorg. Chem. 2000; 39:2273–2278. [PubMed: 12526484]
50. Dhawan IK, Enemark JH. Inorg. Chem. 1996; 35:4873–4882. [PubMed: 11666687]
51. Cooney JA, MAC, Gruhn NE, Joshi HK, Enemark JH. Inorg. Chem. 2004; 43:8110–8118. [PubMed: 15578851]
52. Manuta DM, Lees AJ. Inorg. Chem. 1983; 22:3825–3828.
53. Inscore FE, Knottenbelt SZ, Rubie ND, Joshi HK, Kirk ML, Enemark JH. Inorg. Chem. 2006; 45:967–976. [PubMed: 16441102]
54. Joshi HK, FEI, Schirlin JT, Dhawan IK, Carducci MD, Bill TG, Enemark JH. Inorg. Chim. Acta. 2002; 337:275–286.
55. Joshi HK, Cooney JA, Inscore FE, Gruhn NE, Lichtenberger DL, Enemark JH. Proc. Natl. Acad. Sci. USA. 2003; 100:3719–3724. [PubMed: 12655066]
56. Kapre R, Ray K, Sylvestre I, Weyhermüller T, DeBeer George S, Neese F, Wieghardt K. Inorg. Chem. 2006; 45:3499–3509. [PubMed: 16634580]
57. Nemykin VN, Olsen JG, Perera E, Basu P. Inorg. Chem. 2006; 45:3557–3568. [PubMed: 16634586]
58. Joshi HK, Enemark JH. J. Am. Chem. Soc. 2004; 126:11784–11785. [PubMed: 15382900]

59. Pilato RS, Eriksen K, Greaney MA, Gea Y, Taylor EC, Goswami S, Kilpatrick L, Spiro TG, Rheingold AL, Stiefel EI. ACS Symp. Ser. 1993; 535:83–97.

60. Hsu JK, Bonangolino CJ, Kaiwar SP, Boggs CM, Fettinger JC, Pilato RS. Inorg. Chem. 1996; 35:4743–4751.

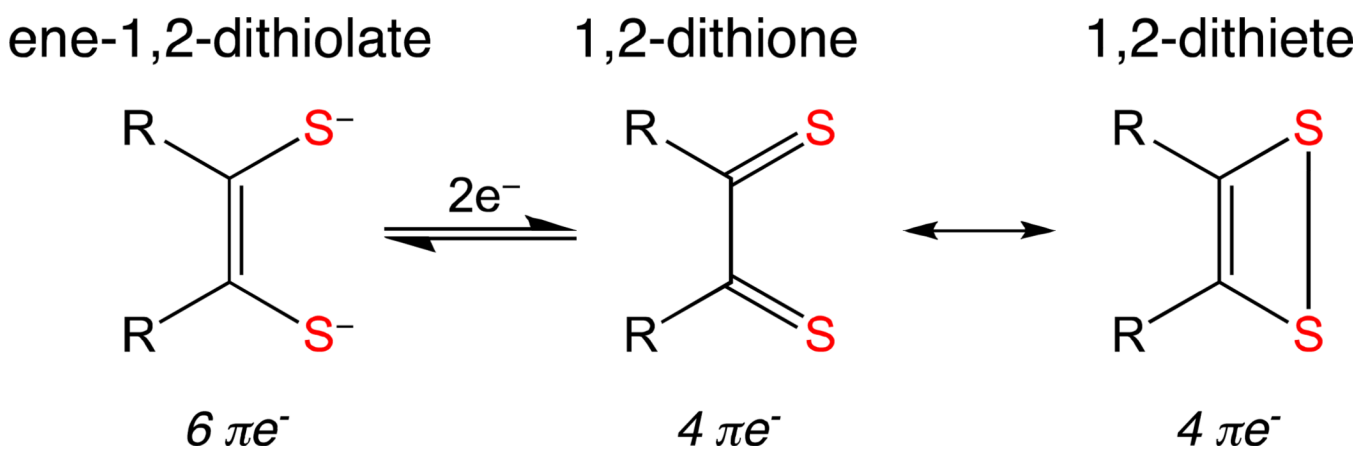

Figure 1.
Valence bond description of dithiolene ligand forms. Two-electron oxidation of the ene-1,2-dithiolate leads to oxidized forms described by 1,2-dithione and 1,2-dithiete Lewis structures.

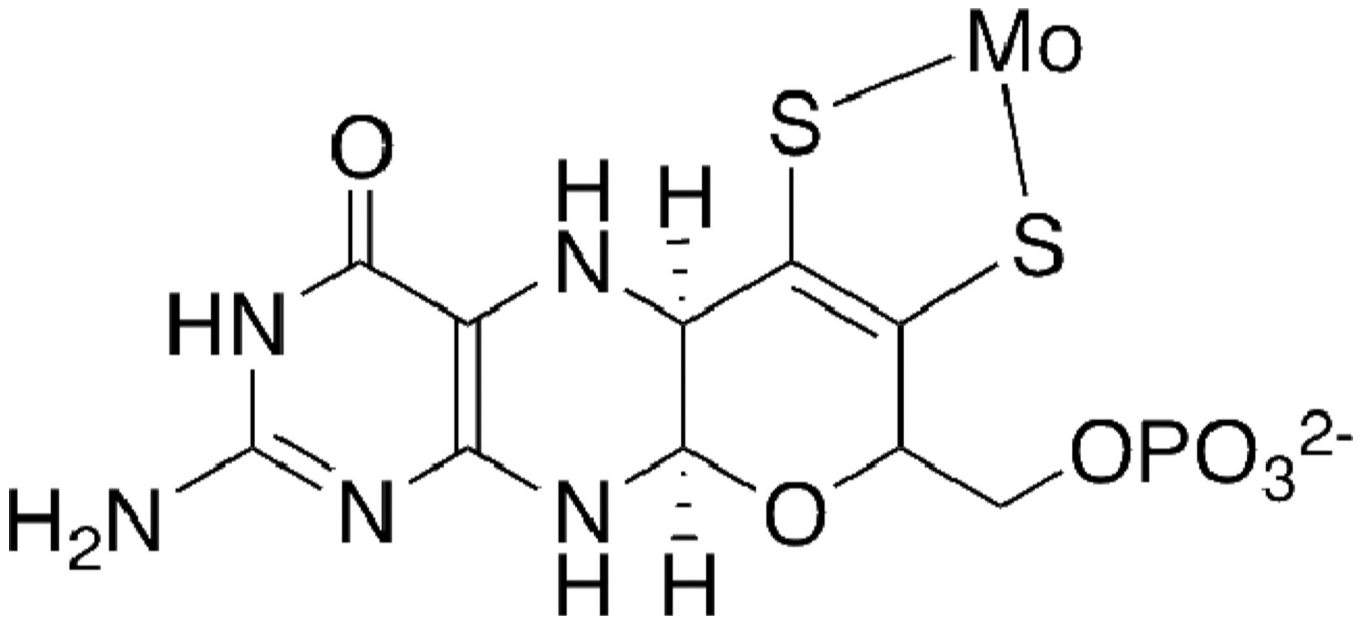

Figure 2.
The pyranopterin dithiolene ligand in the molybdenum cofactor, Moco, the catalytic site in molybdenum enzymes.

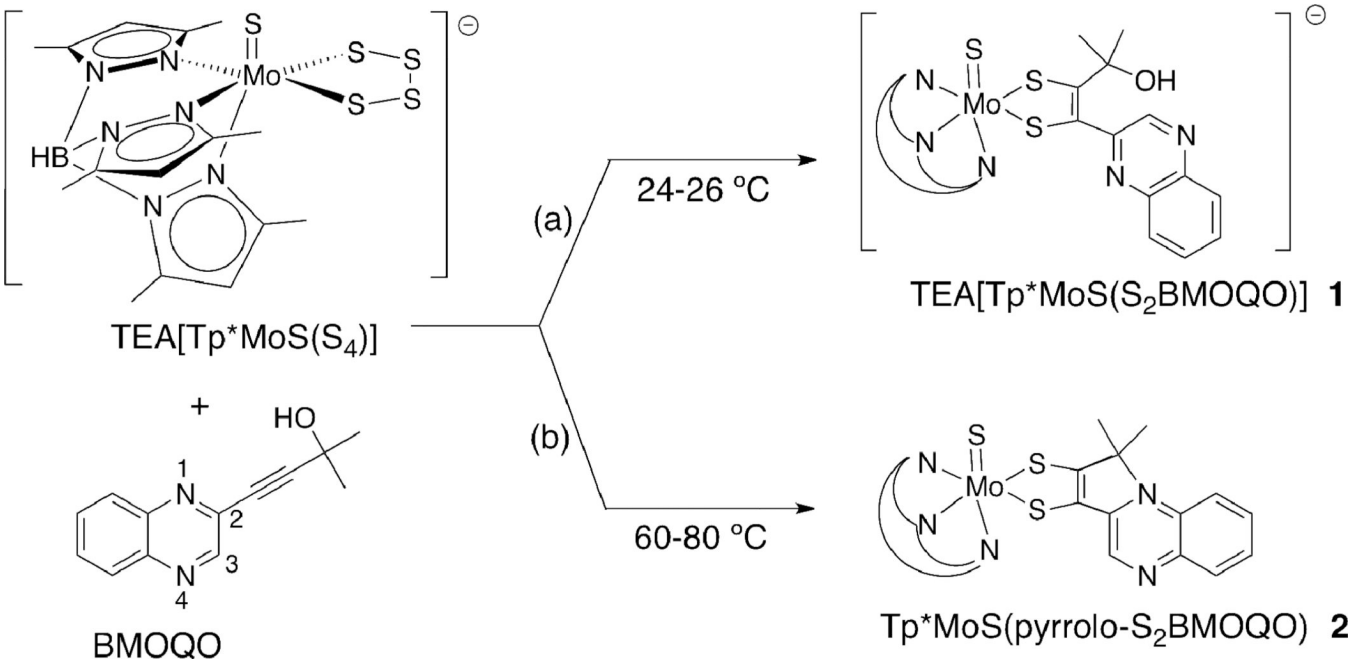

Figure 3.
The reaction of a molybdenum tetrasulfide and an alkyne (BMOQO) forms a quinoxalyldithiolene complex **1** at ambient temperature in path (a) and a pyrroloquinoxalyldithiolene complex **2** under moderate heat in path (b).

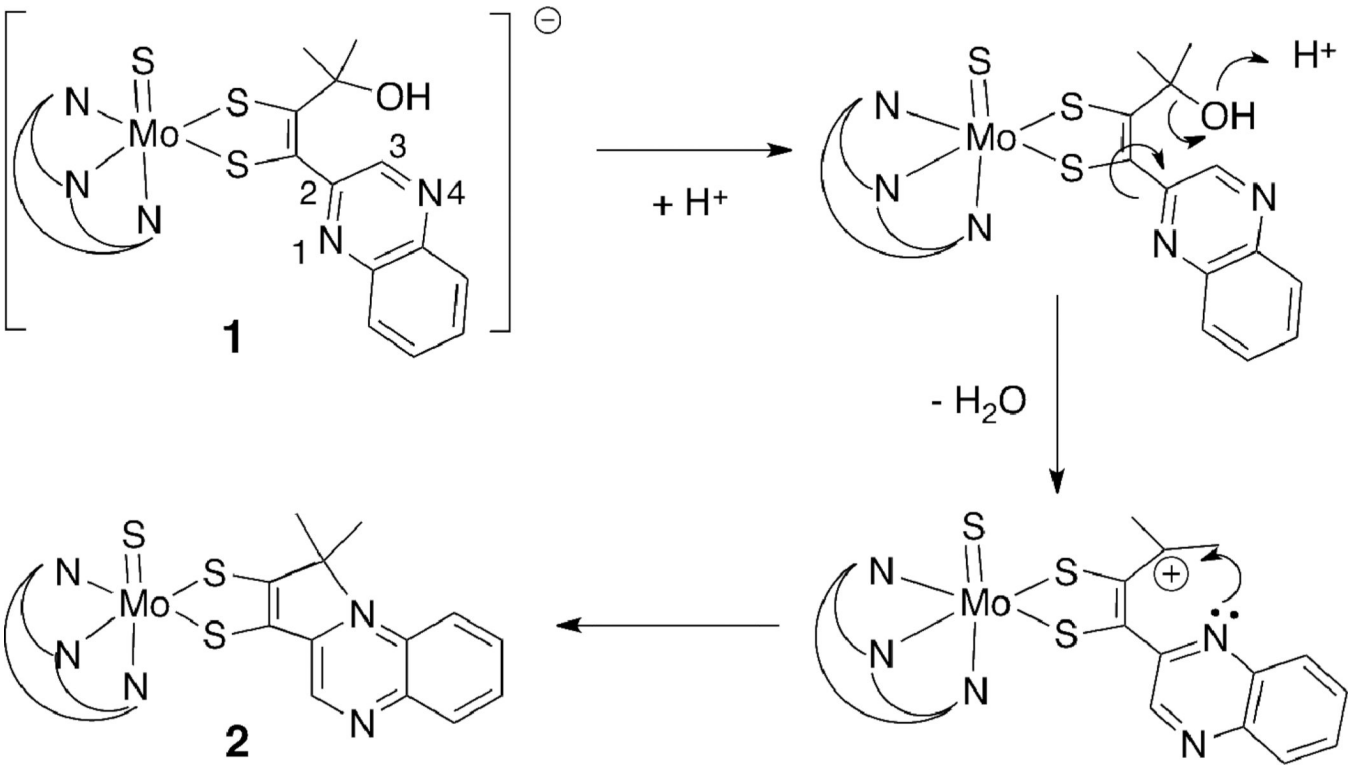

Figure 4.
A proposed mechanism for intramolecular cyclization of complex **1** producing a pyrrolo-dithiolene in **2**.

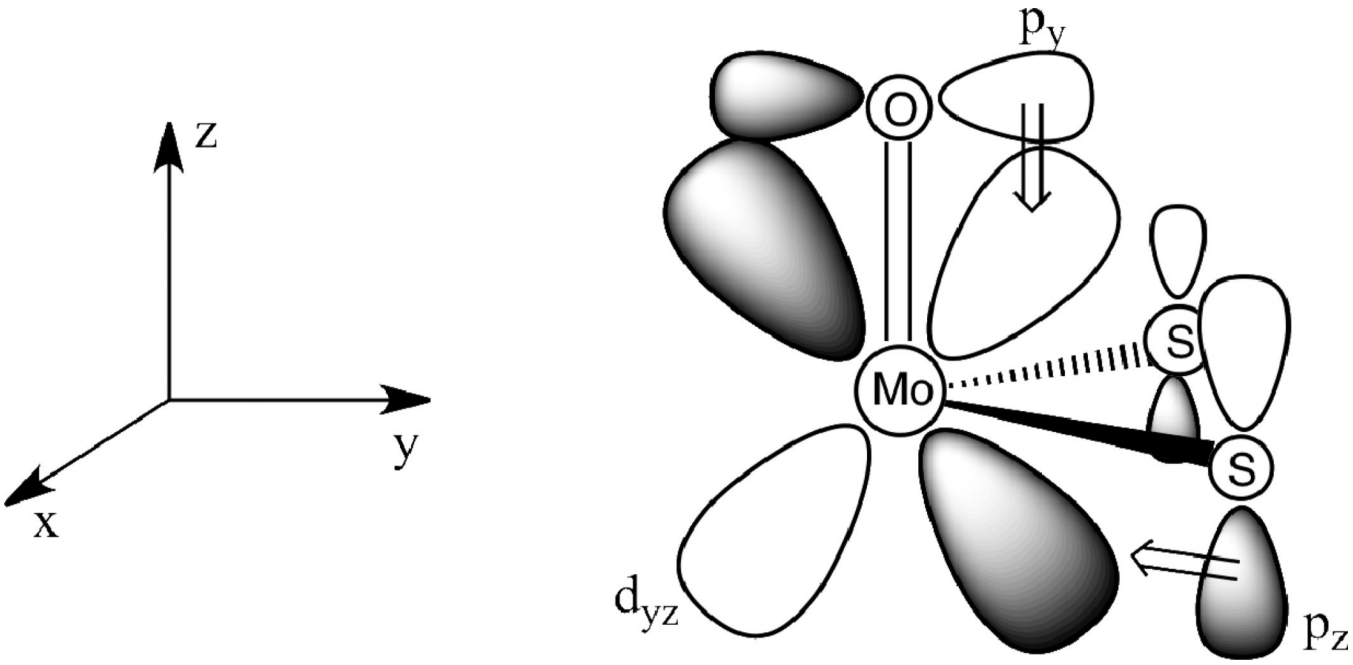

Figure 5.
Competition for π-donation from oxo and dithiolene orbitals to the Mo d_{yz} orbital.

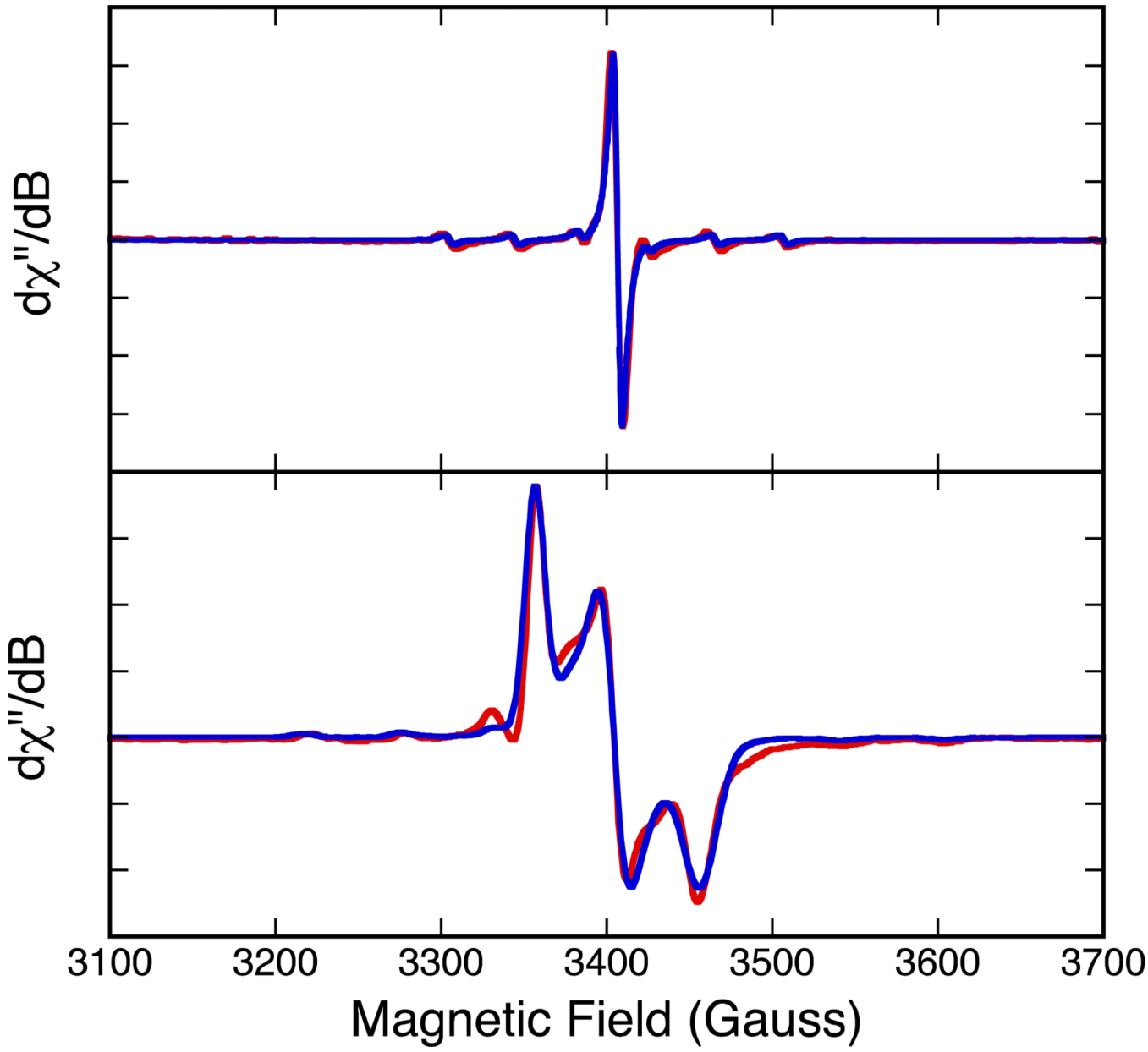

Figure 6.
Top: Room temperature solution isotropic EPR spectrum of **5**. Bottom: 77 K EPR spectrum of **5**. All data were collected in CH_2Cl_2.

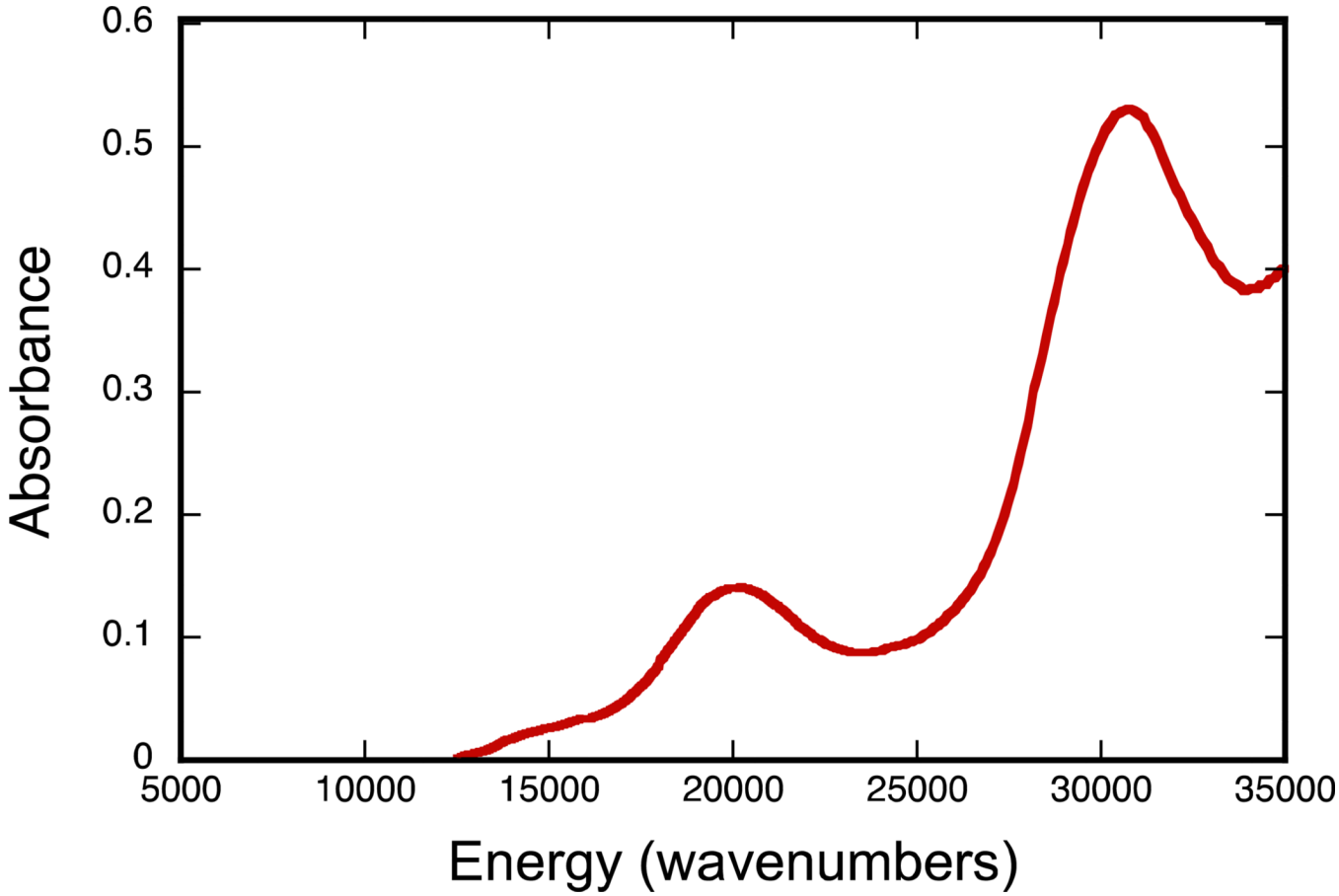

Figure 7.
Electronic spectrum of TEA[Tp*Mo(O)(S_2BMOQO)] **[TEA]3** in acetonitrile with 2% H_2O.

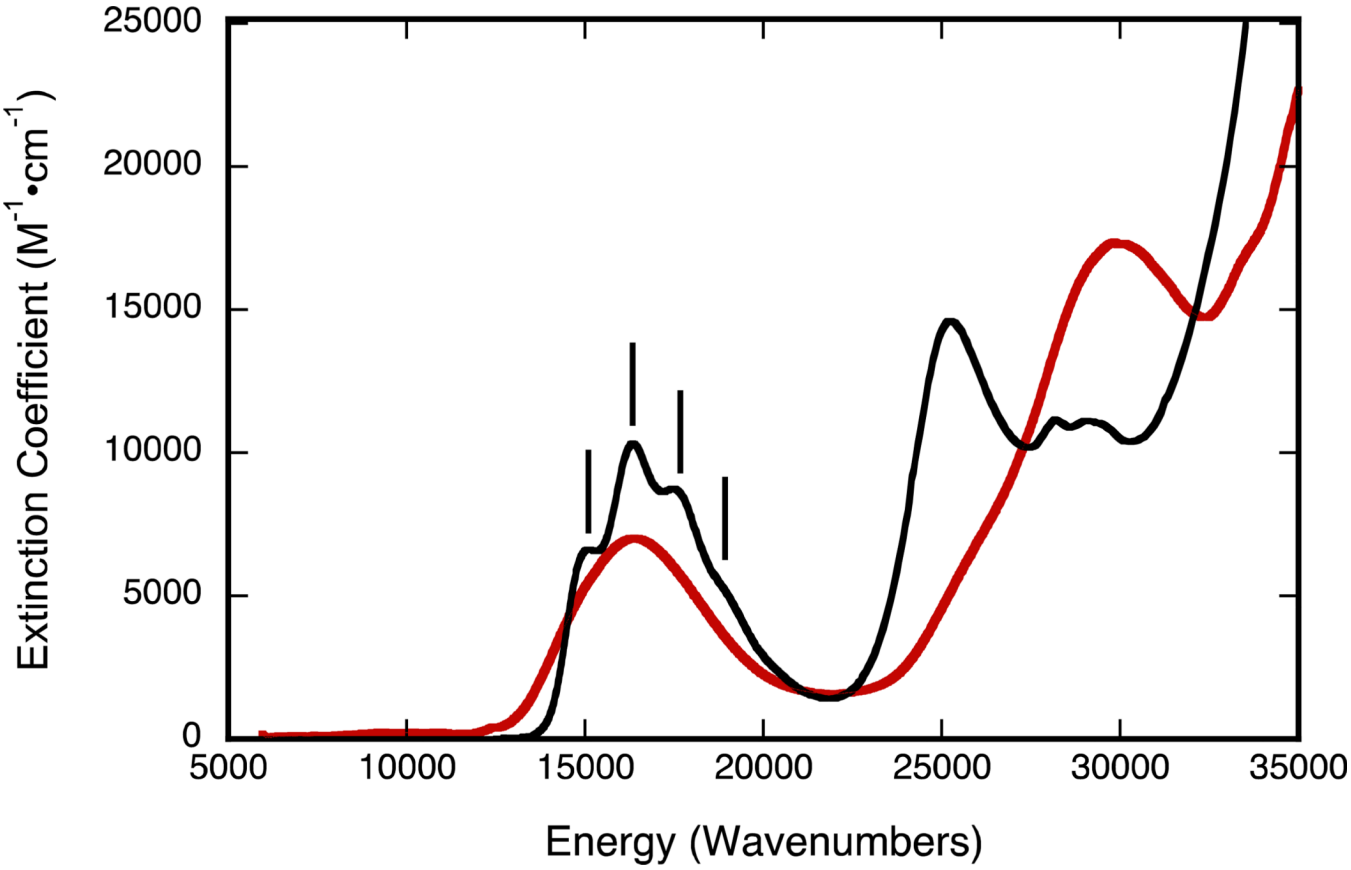

Figure 8.

Electronic spectra of **2** (black line), and **4** (red line) in acetonitrile. $Tp^{*}Mo(S)$(pyrrolo-S_2BMOQO) **2** was hydrolyzed to $Tp^{*}Mo(O)$(pyrrolo-S_2BMOQO) **4** in dichloromethane. Note the apparent vibronic progression (black sticks) built upon the intense visible band of compound **4** with an apparent progression frequency of 1,250 cm^{-1}.

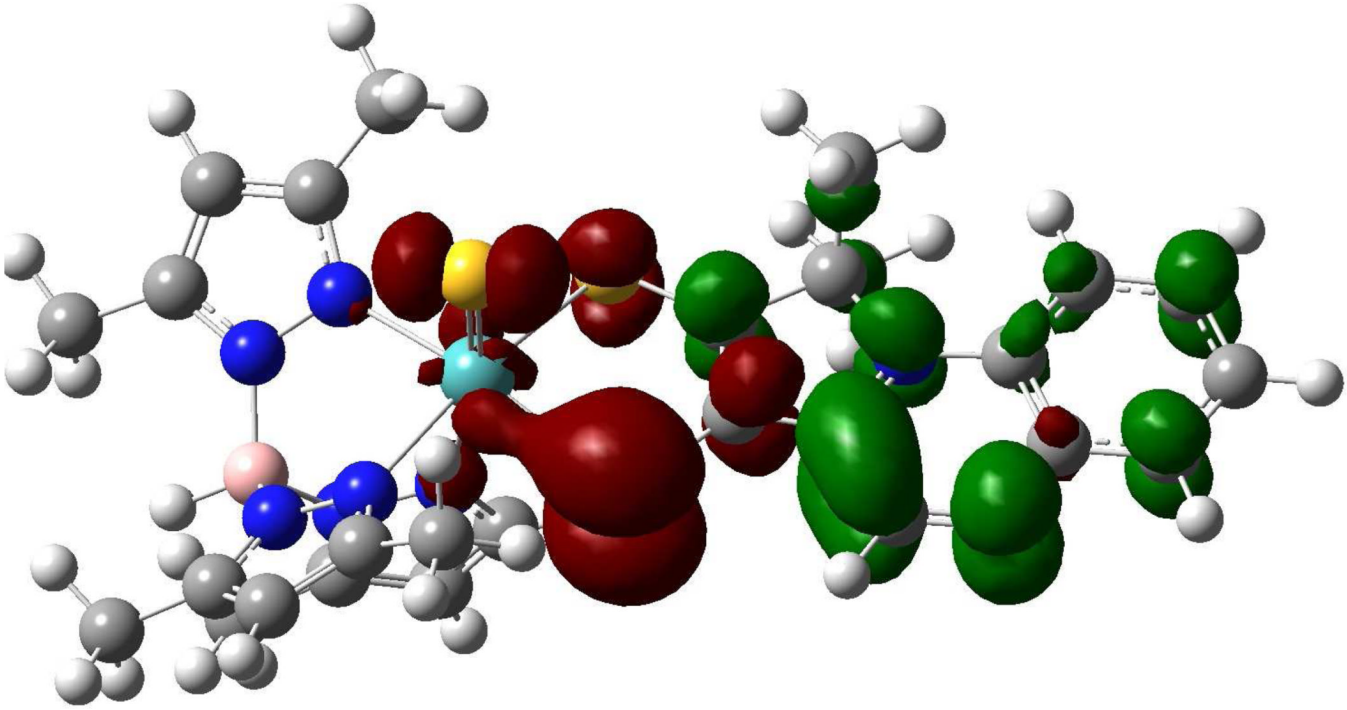

Figure 9.
Calculated electron density difference map that details the nature of the intraligand transition in **2** (red: electron density loss in transition, green: electron density gain in transition.

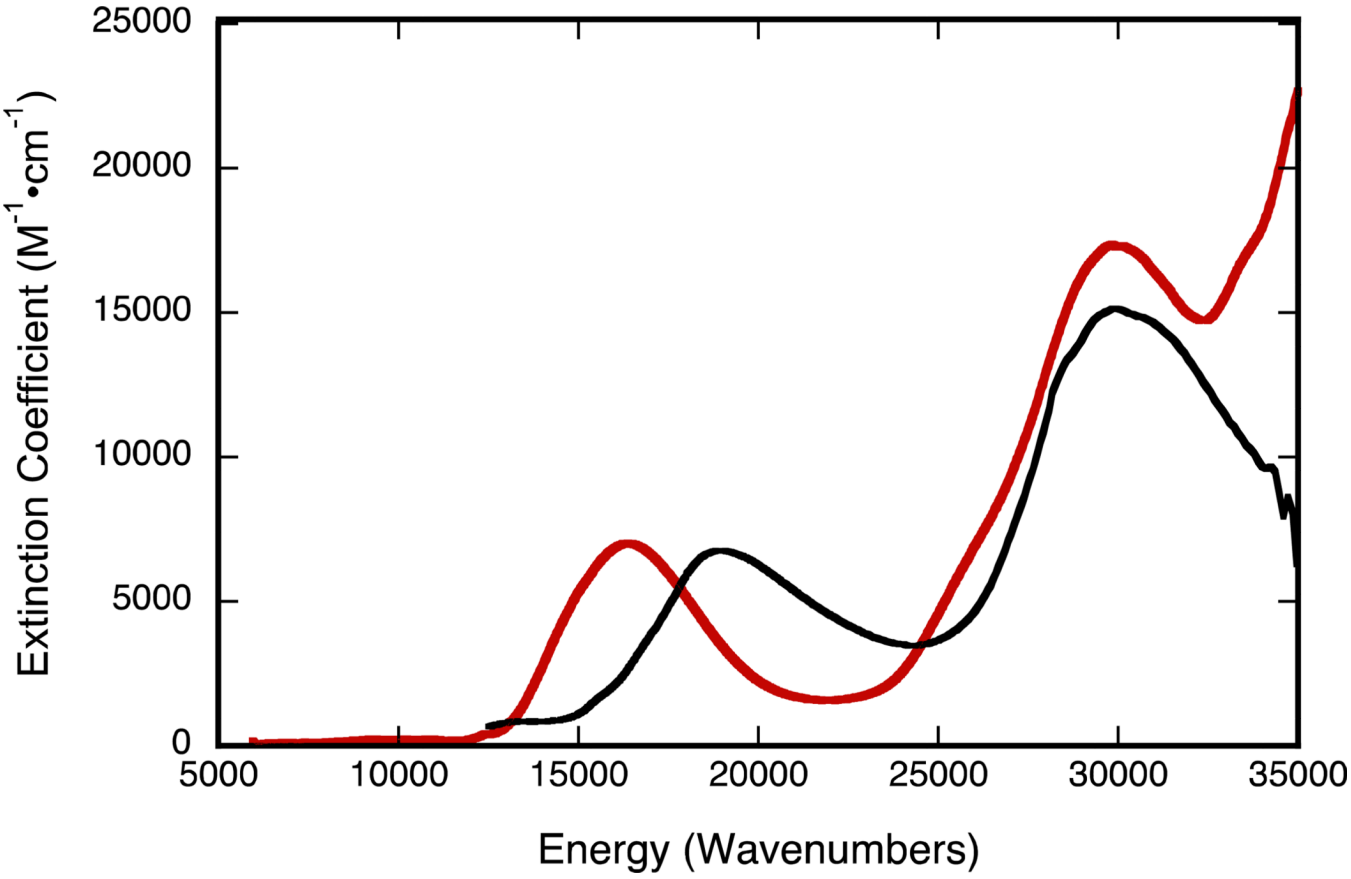

Figure 10.
Electronic spectra of **4** (red line), and **5** (black line) in acetonitrile.

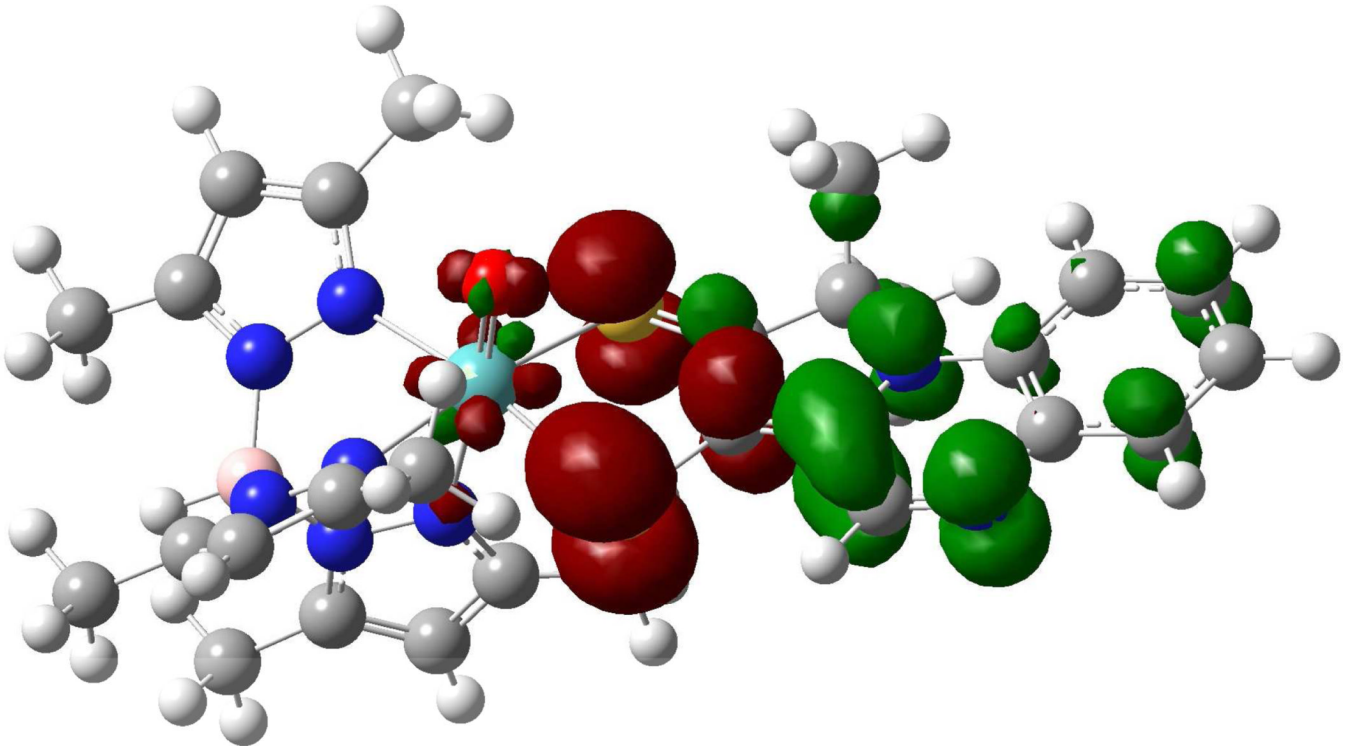

Figure 11.
Calculated electron density difference map that details the nature of the intraligand transition in **5** (red: electron density loss in transition, green: electron density gain in transition.

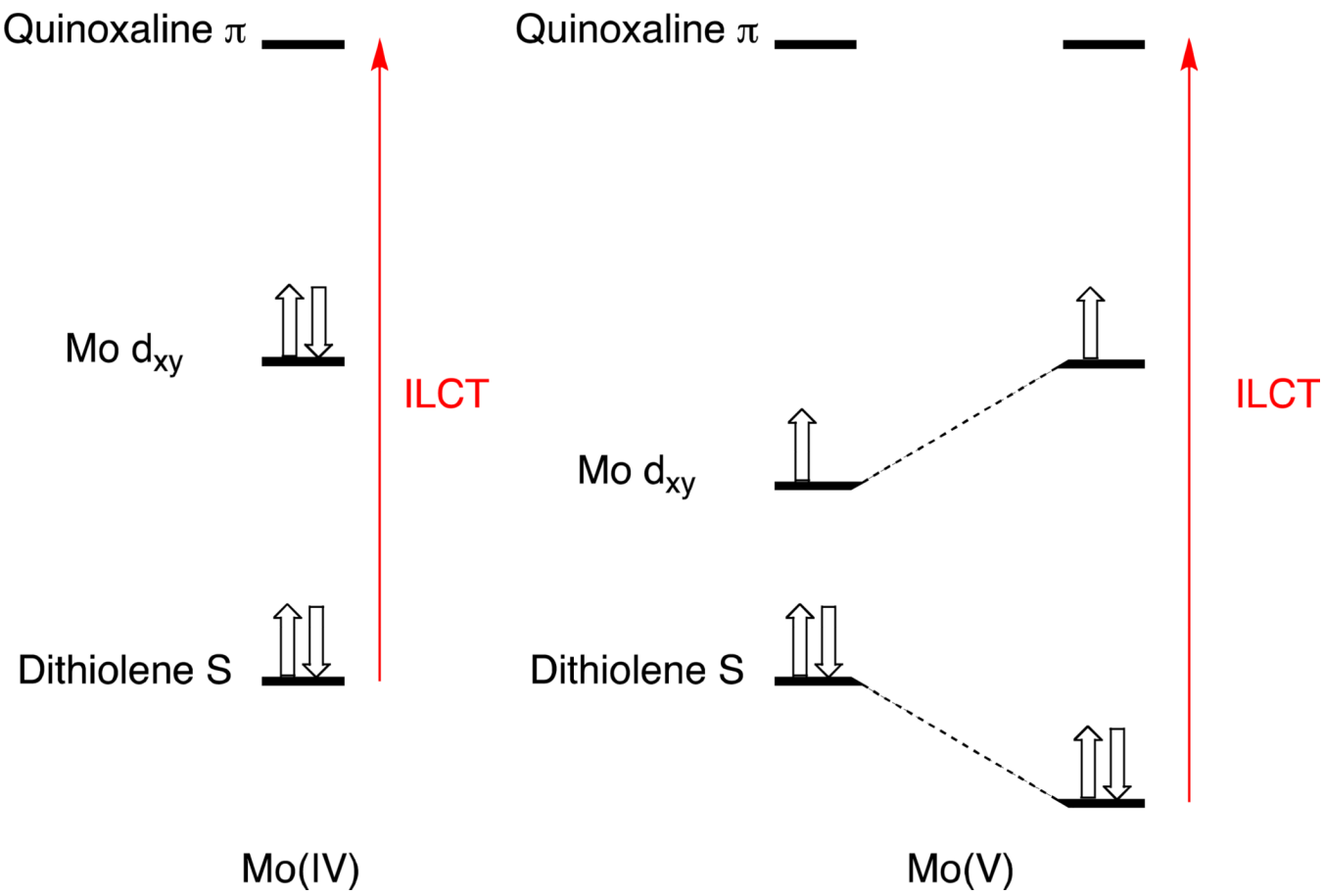

Figure 12.
Qualitative energy level diagram showing how dithiolene S – M d_{xy} interactions in the Mo(5+) state stabilize the dithiolene S donor orbitals and result in a higher energy intraligand CT (ILCT) band in **5** compared with **4**. The d_{x2-y2} orbital is stabilized in Mo(5+) relative to Mo(4+) due to the increased valence ionization energy that results from the increased effective nuclear charge that due to the metal oxidation. Thus, Mo(4+) → Mo(5+) oxidation results in a larger interaction between the metal and ligand orbitals and an increase in dithiolene folding.

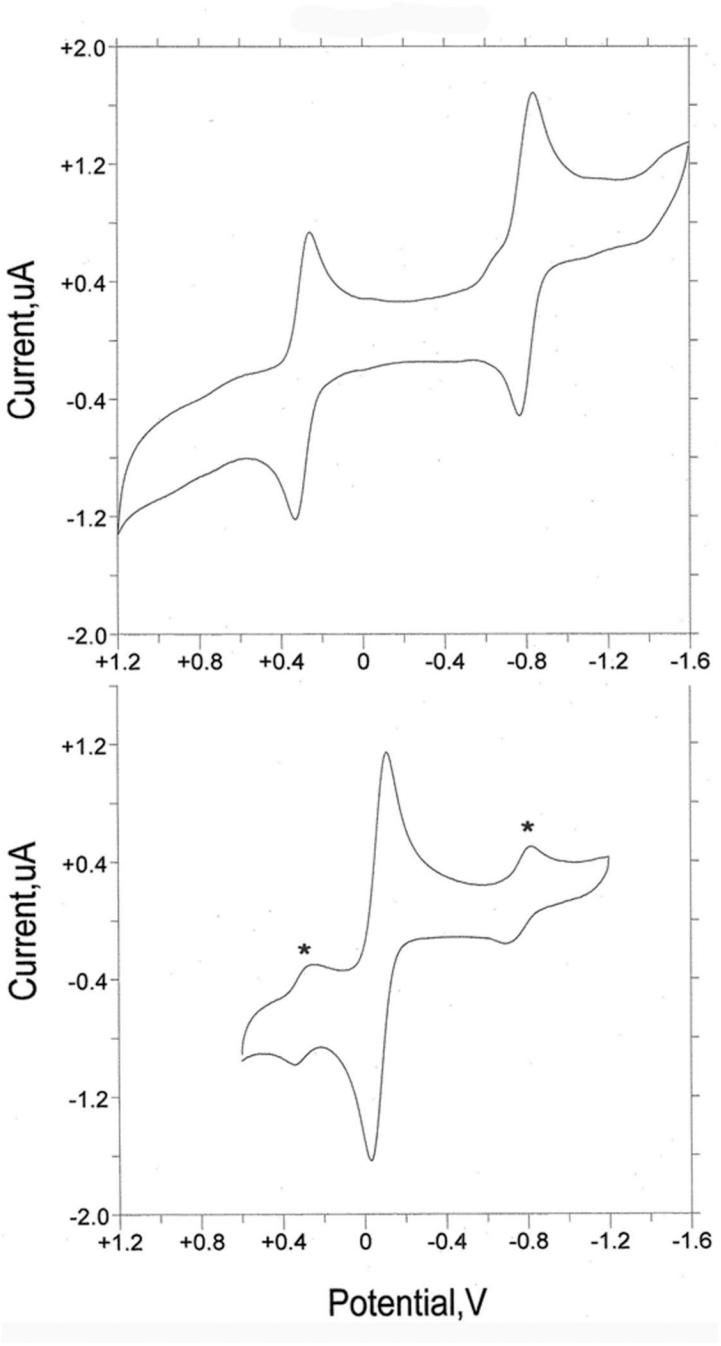

Figure 13.

(*top*) CV of $Tp^{*}Mo(O)$(pyrrolo-S_2BMOQO) **4**. (*bottom*) CV of $[Tp^{*}Mo(O)(S_2BMOQO)]^{-}$ **3** where the asterisks label the signal due to complex **4** formed during the voltammetry experiment. The voltammograms are plotted vs the potential of reference electrode Ag/AgCl in TEAP/ACN.

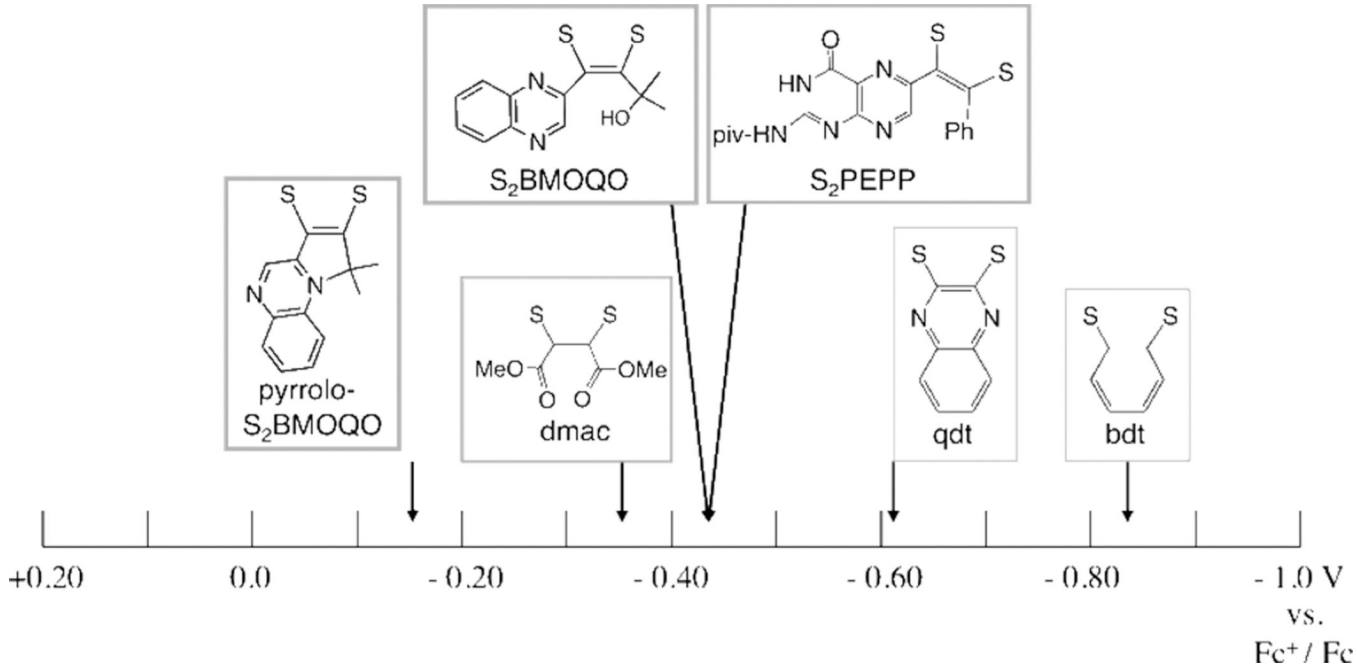

Figure 14.

Mo(5+/4+) reduction potentials for Tp*MoO(dithiolene) complexes in acetonitrile referenced to ferrocenium/ferrocene. Potentials taken from the literature (dithiolene, Mo(5+/4+) V: bdt, −0.84;[49] qdt, −0.62; [49] dmac, −0.35;[44] S_2PEPP, −0.44.[27]

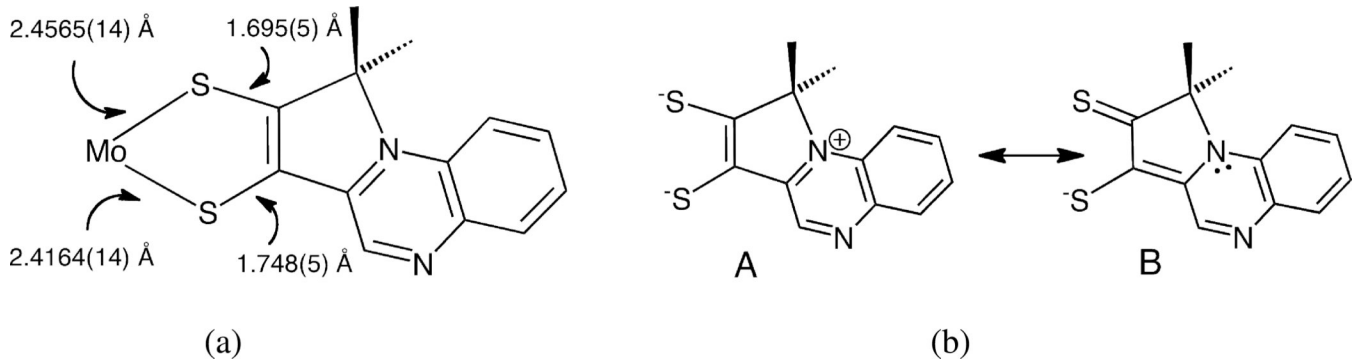

Figure 15.
(a) Asymmetry in bond distances of dithiolene chelate in **4**. (b) Major contributing resonance structures to asymmetric dithiolene in **4**.

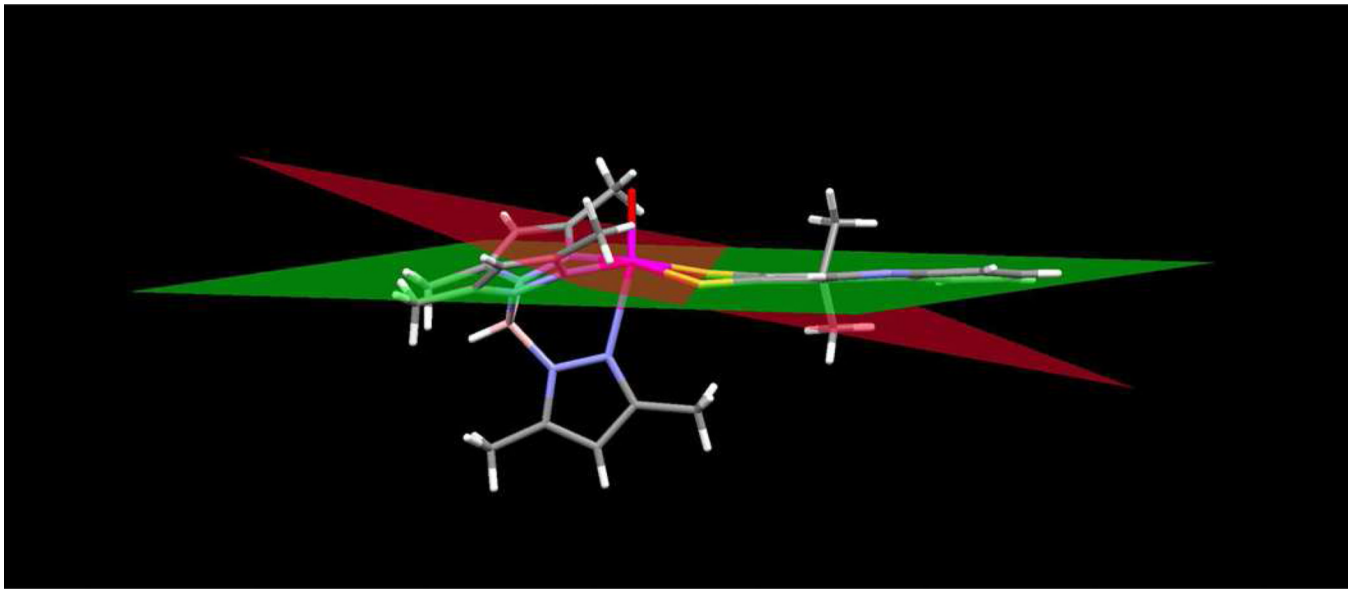

Figure 16.
Dihedral fold angle in **4**. The red plane is calculated through the atoms Mo-S1, S2 of the dithiolene chelate and the green plane is calculated through dithiolene atoms S1, S2, C1 and C2.

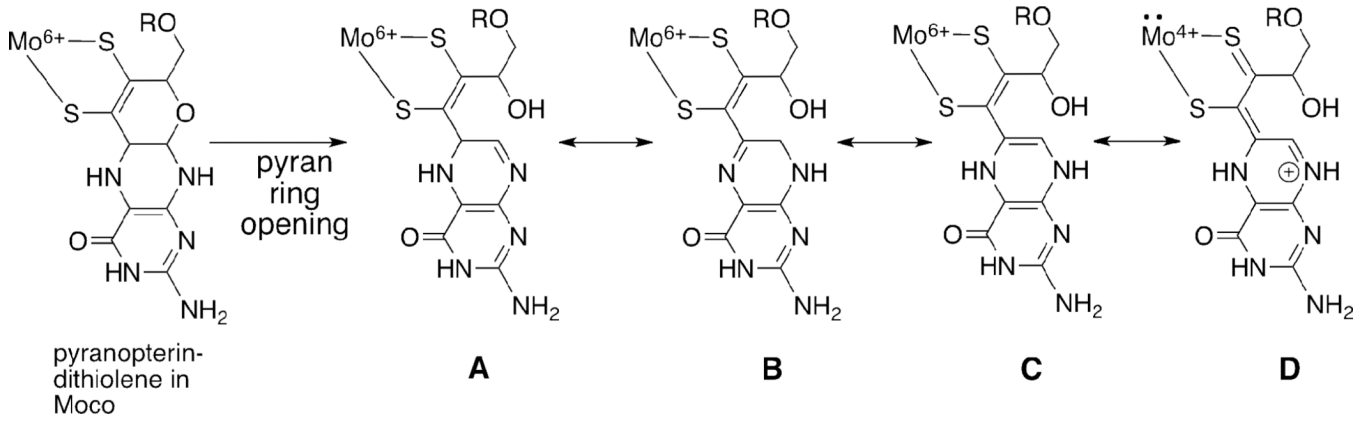

Figure 17.

A pyran ring opening reaction in Moco can generate tautomers A–D by proton migration around the pyrazine ring of the pterin. Valence tautomer D possesses the thione-thiolate chelate form resulting from a formal 2 electron intramolecular redox reaction that produces reduced Mo(4+) and oxidized pterin-dithiolene ligand.

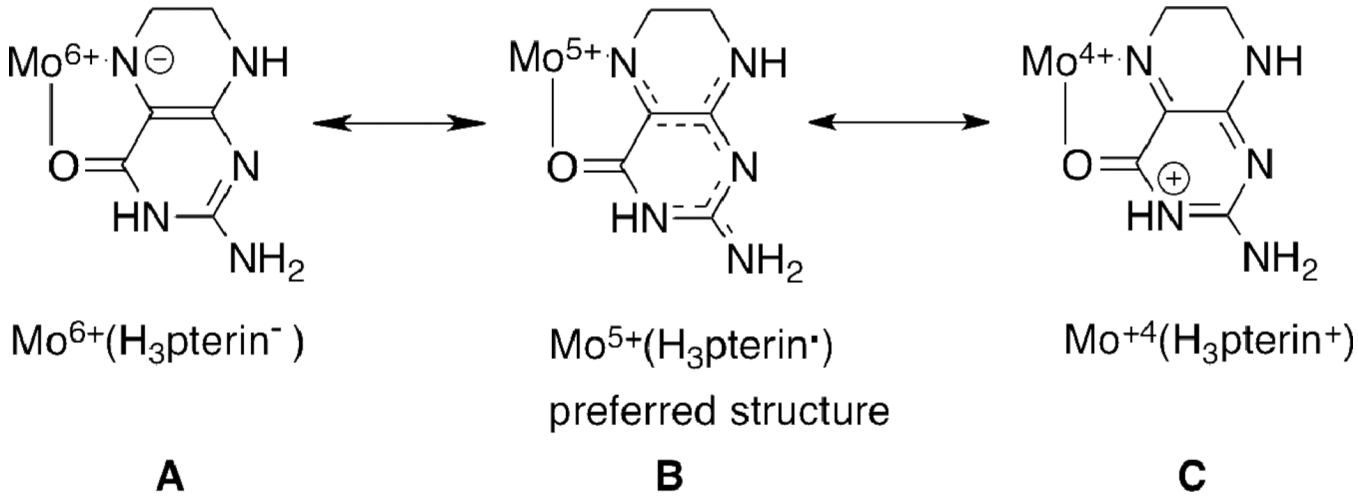

Scheme 1.

Three valence tautomeric structures for reduced pterin chelating Mo illustrating: a deprotonated tetrahydropterin coordinated to Mo(6+) in **A**, a neutral trihydropterin radical coordinated to Mo(5+) in **B** and a protonated dihydropterin coordinated to Mo(4+) in **C**

Table 1

Infrared Data for **1, 2, 3, 4** and **5** and related Tp*Mo(=X)-dithiolene complexes

Compounds reported in this work	$\nu_{Mo=x}$, cm^{-1}	ν_{BH}, cm^{-1}
TEA[Tp*Mo(S)(S_2BMOQO)], **1**	Mo(4+)=S; 496	2520
Tp*Mo(S)(pyrrolo-S_2BMOQO), **2**	Mo(4+)=S; 523	2542
TEA[Tp*Mo(O)(S_2BMOQO)], **3**	Mo(4+)=O; 914	2530
Tp*Mo(O)(pyrrolo-S_2BMOQO), **4**	Mo(4+)=O; 922	2538
[Tp*Mo(O)(pyrrolo-S_2BMOQO)]Cl, **5**	Mo(5+)=O; 935	2545
Related compounds		
TEA[Tp*Mo(S)(S_2DIFPEPP)][27]	Mo(4+)=S; 484	2522
Tp*Mo(S)(S_2DIFPEPP)[27]	Mo(5+)=S; 493	2545
TEA[Tp*Mo(O)(S_2DIFPEPP)][27]	Mo(4+)=O; 922	2522
Tp*Mo(O)(S_2DIFPEPP)[27]	Mo(5+)=O; 929	2545
Tp*Mo(S)(S_2DMAC)[44]	Mo(5+)=S; 490	Not reported
Tp*Mo(O)(S_2DMAC)[44]	Mo(5+)=O; 935	2563
Tp*Mo(O)(tdt)[49]	Mo(5+)=O; 926	Not reported
Tp*Mo(O)(bdt)[49]	Mo(5+)=O; 932	Not reported
Tp*Mo(O)(qdt)[49]	Mo(5+)=O; 940	2551

DIFPEPP is 1,2,-(2,4-difluorophenyl)(pterinyl)dithiolene); DMAC is dimethylcarboxyacetylene; bdt is 1,2-benzene dithiolate, tdt is toluenedithiolate, qdt is 2,3-quinoxalinedithiolate.

Table 2

Electronic spectral data for oxo- and sulfido-molybdenum dithiolene compounds.

Dithiolene complex	λ, nm (ε, $M^{-1}cm^{-1}$)
$[Tp^{*}Mo(O)(S_2BMOQO)]^{-}$ **3**	~340, ~490
$Tp^{*}Mo(4+)(O)$(pyrrolo-S_2BMOQO) **4**	336 (13,150), 610 (5190), 1024 (250)
$Tp^{*}Mo(S)$(pyrrolo-S_2BMOQO) **2**	390 (11,765), 527 (5089), 566 (8598), 606 (10,120), 661(6612)
$[Tp^{*}Mo(5+)(O)$(pyrrolo-S_2BMOQO)]+ **5**	335 (15,143), 528 (6582)
Tp*Mo(5+)O(S_2DMAC)	437 (2850), 590 (708), 1125 (385)
$Tp^{*}Mo(5+)(O)$(tdt)	403 (5491), 510 (1324), 767 (274), 1100 (490)
$Tp^{*}Mo(5+)(O)$(qdt)	389 (4027), 523 (1050), 729 (130), 885 (170)

Table 3

A Comparison of Solvent Polarity and Wavelength in Increasingly Polar Solutions of Tp*Mo(O)(pyrrolo-S_2BMOQO) **4**.

Solvent	Abs_{max}, nm	Dielectric Constant, ε	E^*_{MLCT}[52]	Solvent parameter[12]
Toluene	653	2.38	0.30	0.172
Diethyl Ether	648	4.33	0.32	---
Chloroform	615	4.81	0.42	0.61
Acetone	600	20.7	0.82	0.797
Ethanol	600	24.5	0.69	---
Methanol	596	32.7	0.73	---
Dimethylsulfoxide	596	46.7	1.00	0.973

Table 4

Electrochemical data for oxo- and sulfido-molybdenum quinoxalyl- and pterinyl dithiolene compounds

Dithiolene compound	**E($Mo^{5/4}$),V**	**ΔE_{pp}, V**	**i_a/i_c**	**E(L), V**	**ΔE_{pp}, V**	**i_a/i_c**
$[Tp^*Mo(O)(S_2BMOQO)]^-$ **3**	−0.43					
$Tp^*Mo(O)$(pyrrolo-S_2BMOQO) **4**	−0.15	60	0.99	−1.25	62	0.85
$Tp^*Mo(S)$(pyrrolo-S_2BMOQO) **2**	−0.35	55	0.59	−1.58	62	0.88
Tp*MoO(S_2DIFPEPP)[27]	−0.44	70	0.93			
Tp*MoS(S_2DIFPEPP)[27]	−0.58	60	0.97			
Tp*MoO(S_2PEPP)[27]	−0.43	68	1.0			
Tp*MoS(S_2PEPP)[27]	−0.59	78	1.0			

All potentials referenced to internal ferrocene whose potential is +0.40 vs. the Ag/AgCl reference electrode. ACN, acetonitrile. S_2DIFPEPP is 1,2,-(2,4-difluorophenyl)(pterinyl)dithiolene); S_2PEPP is 1,2,-(phenyl)(pterinyl)dithiolene)